Cardiomyocyte-specific RXFP1 overexpression protects against pressure overload-induced cardiac dysfunction independently of Relaxin

J. Wingert, E. Meinhardt, N. Sasipong, M. Pott, C. Lederer, C. de la Torre, C. Sticht, P. Most, H. A. Katus, N. Frey, Philip Raake, P. Schlegel
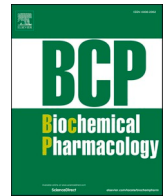
Cardiomyocyte-specific RXFP1 overexpression protects against pressure overload-induced cardiac dysfunction independently of relaxin

J. Wingert [a,b], E. Meinhardt [a], N. Sasipong [a], M. Pott [a], C. Lederer [c], C. de la Torre [d], C. Sticht [d], P. Most [a,b], H.A. Katus [a,b], N. Frey [a,b], P.W.J. Raake [a,b,e], P. Schlegel [a,b,*]

[a] Department of Internal Medicine III, Cardiology, University Hospital Heidelberg, Heidelberg University, Germany
[b] DZHK (German Centre for Cardiovascular Research), partner site Heidelberg/Mannheim, Germany
[c] Thoraxklinik Heidelberg, University Hospital Heidelberg and German Center for Lung Research (DZL), Heidelberg, Germany
[d] Core Facility Platform Mannheim, NGS Core Facility, Medical Faculty Mannheim, Heidelberg University, Mannheim, Germany
[e] Department of Internal Medicine I, University Hospital Augsburg, Augsburg University, Germany

ARTICLE INFO

ABSTRACT

Heart failure (HF) prevalence is rising due to reduced early mortality and demographic change. Relaxin (RLN) mediates protective effects in the cardiovascular system through Relaxin-receptor 1 (RXFP1). Cardiac overexpression of RXFP1 with additional RLN supplementation attenuated HF in the pressure-overload transverse aortic constriction (TAC) model. Here, we hypothesized that robust transgenic RXFP1 overexpression in cardiomyocytes (CM) protects from TAC-induced HF even in the absence of RLN.

Hence, transgenic mice with a CM-specific overexpression of human RXFP1 (hRXFP1tg) were generated. Receptor functionality was demonstrated by *in vivo* hemodynamics, where the administration of RLN induced positive inotropy strictly in hRXFP1tg. An increase in phospholamban-phosphorylation at serine 16 was identified as a molecular correlate. hRXFP1tg were protected from TAC without additional RLN administration, presenting not only less decline in systolic left ventricular (LV) function but also abrogated LV dilation and pulmonary congestion compared to WT mice. Molecularly, transgenic hearts exhibited not only a significantly attenuated fetal and fibrotic gene activation but also demonstrated less fibrotic tissue and CM hypertrophy in histological sections. These protective effects were evident in both sexes. Similar cardioprotective effects of hRXFP1tg were detectable in a RLN-knockout model, suggesting an alternative mechanism of receptor activation through intrinsic activity, alternative endogenous ligands or crosstalk with other receptors.

In summary, CM-specific RXFP1 overexpression provides protection against TAC even in the absence of endogenous RLN. This suggests RXFP1 overexpression as a potential therapeutic approach for HF, offering baseline protection with optional RLN supplementation for specific activation.

1. Introduction

Heart failure (HF) affects more than 64 million people worldwide and its prevalence is rising due to demographic transition and reduced early mortality [1], resulting in a growing social and economic burden [1] and a need for novel effective therapies.

Serelaxin, the recombinant form of the peptide hormone relaxin (RLN), was considered such a potential breakthrough therapy for acute heart failure. Through binding to Relaxin-receptor 1 (RXFP1), the hormone RLN, designated H2 RLN in humans and M1 RLN in mice, exerts vasodilatory, anti-fibrotic, anti-apoptotic, anti-inflammatory, and positive inotropic effects in the cardiovascular system [2]. RLN has proven to be a potent vasodilator *in vitro* [3] and to reduce vascular resistance and increase large artery compliance *in vivo* in distinct rodent models [4,5]. Anti-fibrotic RLN effects *in vitro* were demonstrated in rat atrial and ventricular fibroblasts [6], *in vivo* antifibrotic RLN effects in the heart were detectable in various rodent models of myocardial ischemia [7–9], in spontaneously hypertensive rats [10,11] and aged rats [12–14]. The latter group also provided insights into the beneficial electrophysiological and anti-arrhythmic effects of RLN in myocardium [15]. Inversely, RLN-knockout mice have been reported to develop increased cardiac fibrosis and ventricular chamber stiffness [16]. Anti-apoptotic RLN effects were demonstrated *in vitro* for oxidative stress [17], high glucose [18] and hypoxia-reoxygenation [19] and *in vivo* in a rodent model of myocardial infarction by LAD ligation [9]. Furthermore, RLN produced positive inotropic effects in atrial but not in ventricular myocardium [20]. These promising data on the potential therapeutic properties of RLN paved the way for evaluation in humans.

In a first dose-escalation clinical trial, RLN produced favorable hemodynamic effects in patients with stable systolic HF [21]. This could be confirmed in a subsequent clinical trial in patients with acute heart failure (aHF) [22]. These effects comprised a significant decrease in peak pulmonary artery wedge pressure, right atrial pressure, and systemic/pulmonary vascular resistance along with improved renal function [22]. The effects of a continuous 48-hour Serelaxin infusion on aHF were further evaluated in the RELAX-AHF phase 3 trials [23,24]. RELAX-AHF met the primary endpoint of dyspnea-reduction and implied a reduced 180-day mortality in patients receiving Serelaxin [24]. However, RELAX-AHF-2 could not validate these findings [23]. This outcome may have been attributed to the short half-life of RLN [25] and/or the absence of its cognate receptor, RXFP1, in ventricular CMs [20,26]. Given RLN's protective profile and the outcomes of the clinical trials, we hypothesized that amplifying ventricular RXFP1 expression could enhance the leverage of RLN's effects.

Vector-based RXFP1 overexpression in CMs along with RLN administration restored left ventricular (LV) systolic function and reduced pathological remodeling in mice subjected to pressure overload by transverse aortic constriction (TAC) [26]. However, there were no clear indications of significant differences in typical RLN signaling aspects, such as fibrosis attenuation [26]. Yet, even without additional RLN administration, vector-based RXFP1 overexpression showed a trend towards attenuated HF development [26] and protected against acute myocardial infarction [27]. This raises questions about whether isolated RXFP1 overexpression alone could suffice to attenuate HF, the potential role of endogenous RLN in this scenario, and its impact on fibrosis. Therefore, this study was designed to investigate whether transgenic mice with robust CM-specific RXFP1 overexpression are shielded from HF and to evaluate the relevance of endogenous RLN in this context.

2. Materials and methods

2.1. Ethics statement

All animal procedures and experiments were performed in accordance with the Guide for the Care and Use of Laboratory Animals (National Institutes of Health [NIH]) and approved by the Regierungspräsidium Karlsruhe, Baden-Württemberg, Germany (reference numbers G-52/16, G-261/17, G-217/20, G-260/21).

2.2. Generation of hRXFP1tg mice

Human RXFP1 cDNA (GenBank: NM_021634.3) with a FLAG-tag was synthesized and cloned into an empty backbone plasmid containing an α-MHC Promotor (pJG/ALPHA MHC), where it was inserted between promotor and hGH polyA sequence (Fig. 1A).

Microinjection of the genetic construct into the pronuclei of fertilized eggs and oviduct transfer of the embryos into pseudopregnant surrogate mothers (C57Bl/6NCrl strain) was performed at the Interfaculty Biomedical Facility at the University of Heidelberg. DNA was isolated from ear biopsies of 3-week-old offspring using a DNeasy Blood & Tissue Kit (Qiagen, Hilden, Germany). The number of transgene copies per genome was quantified against a reference standard series using a SYBR-green quantitative real-time polymerase chain reaction (qRT-PCR) assay (Bio-Rad, Munich, Germany) as described in section 2.11. Transgenic mice were mated with wildtype (WT) mice for two generations to achieve strains with stable transgene copy numbers. Mice with 200 and 100 transgene copies per heterozygous genome were chosen as founders for these experiments hereinafter denoted hRXFP1tg_high (200 copies) and hRXFP1tg_low (100 copies). Sanger sequencing of the transgene was performed to verify correct transgene integration.

2.3. Immunohistochemical FLAG-staining

Immunohistochemical (IHC) FLAG-staining of representative formalin-fixed paraffin-embedded LV specimens was performed by the Center for Model System and Comparative Pathology at the University of Heidelberg using a FLAG antibody (mouse monoclonal; Sigma-Aldrich, Cat. F1804) according to standard protocols. Images were acquired at 20-fold magnification using a Hamamatsu NanoZoomer Digital Pathology system (Hamamatsu Photonics, Hamamatsu, Japan).

2.4. Preparation of histological samples

Ventricular tissue specimens were fixed in 4 % Paraformaldehyde (PFA) in PBS (pH 7.4, MORPHISTO GmbH, Offenbach, Germany), dehydrated using a HistoCore Pearl (Leica, Wetzlar, Germany) in ascending concentrations of alcohol, xylene, and paraffin, and eventually embedded in paraffin using a Leica HistoCore Arcadia Station. 5 μm thick tissue sections were prepared using a Leica RM2145 Microtome.

2.5. Masson-trichrome staining

Masson Trichrome Staining was performed using a Masson Trichrome Staining Kit (HT15, Sigma Aldrich, Munich, German). Upon evaporation of xylene, the sections were embedded using standard mounting medium (O.Kindler, Bobingen, Germany).

2.6. Picrosirius red staining

Following Masson Trichrome Staining, the sections were incubated in Picrosirius Red (PSR, Scy Tek, Utah, USA) solution for 15 min, rinsed three times in 1 % acetic acid and incubated in 1 % acetic acid for 2 min, and eventually dehydrated (70 % EtOH, 96 % EtOH, 100 % EtOH, 100 % Xylene, 1 min each). Upon evaporation of xylene, the sections were embedded using standard mounting medium (O.Kindler, Bobingen, Germany).

Sections were visualized using a Zeiss Axio Observer inverted fluorescence microscope (Carl Zeiss, Oberkochen, Germany) in the Texas Red and FITC channel [28]. Interstitial fibrosis in 10 images per animal was quantified using ImageJ (v1.54f) and averaged. The macro code is available upon request.
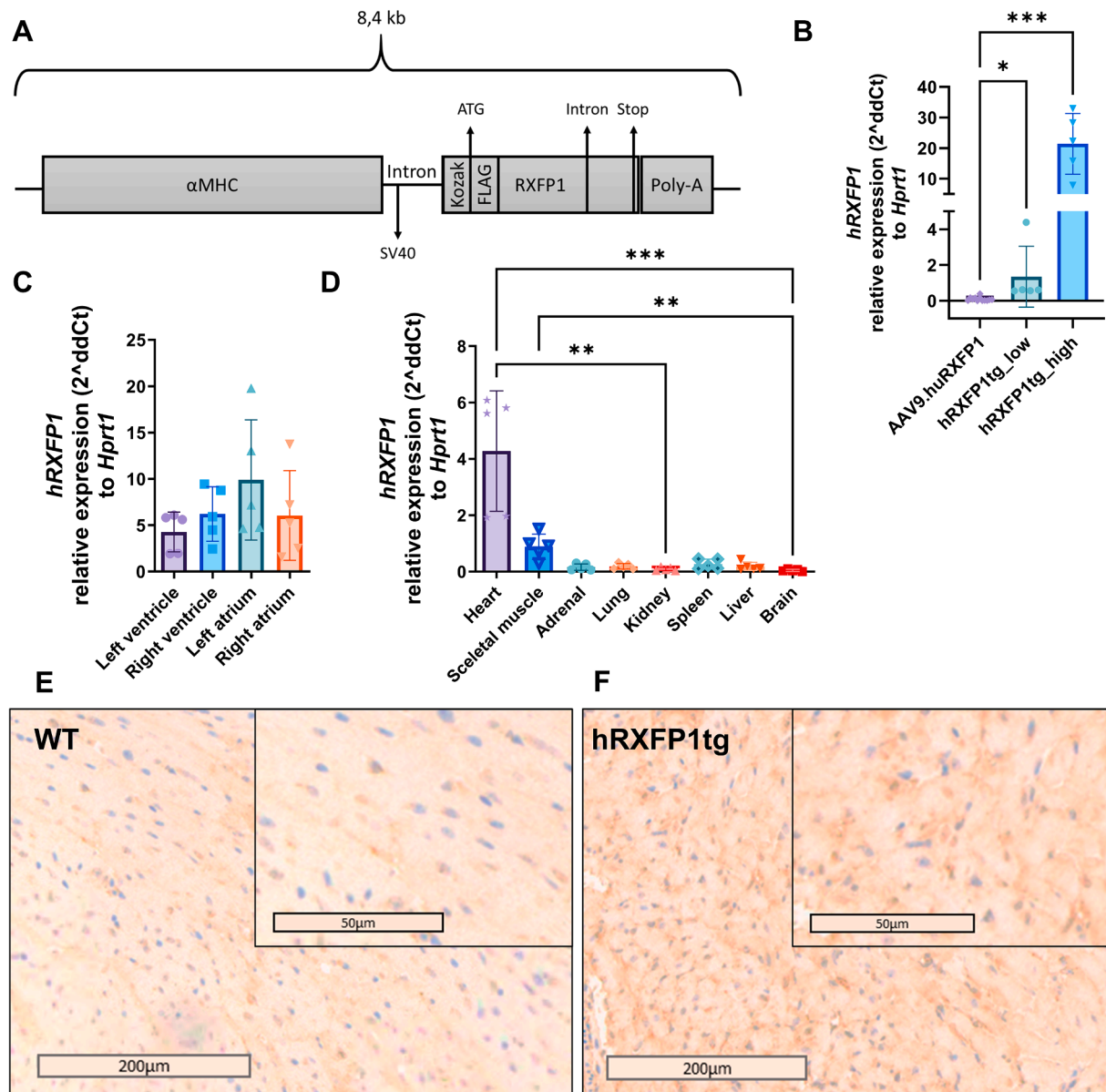
Fig. 1. Generation and characterization of hRXFP1tg mice. (A) Genetic construct used for generation of hRXFP1tg mice. (B) hRXFP1 mRNA expression in the LV 7 weeks after AAV9.huRXFP1 virus administration compared to hRXFP1tg_high and hRXFP1tg_low mice. n = 5 hRXFP1tg_high / 4 hRXFP1tg_low / 12 AAV9.huRXFP1. (C)-(D) hRXFP1tg mRNA expression in distinct heart chambers (C) and organs (D) of hRXFP1tg_low mice. n = 5 per group. (E)–(F) Immunohistochemical FLAG-tag staining in left ventricles; scale bar 200 μm and 50 μm; (E) WT and (F) hRXFP1tg. Significant differences in (B)-(D) were determined by Kruskal-Wallis one-way ANOVA test with Dunn's multiple comparison test. Values represent the mean ± SD; * − p ≤ 0.05; ** − p ≤ 0.01; *** − p ≤ 0.001.

2.7. Wheat germ agglutinin staining

Tissue sections were deparaffinized, rehydrated (20 min 100 % Xylene, 4 min 100 % EtOH, 4 min 96 % EtOH, 4 min 70 % EtOH), washed in H2Odd, and incubated at ∼ 95 °C in sodium citrate solution (2 mM citric acid, 9 mM trisodium citrate, pH 6) and then washed 3 times for 2 min in HBSS. Sections were incubated in 100 μl WGA/DAPI solution (10 μg/ml WGA Alexa Fluor 488 conjugate (ThermoFisher Scientific, Dreieich, Germany), 5 μg/ml DAPI (ThermoFisher Scientific, Dreieich, Germany) in HBSS) for 20 min at room temperature. The slides were washed for 3x2 min in HBSS. Slides were covered in VECTASHIELD Antifade Mounting Medium (Vector Laboratories, Newark CA, USA) and allowed to harden at 4 °C.

Sections were visualize using a Zeiss Axioscan 7 slide scanner (Carl Zeiss, Oberkochen, Germany) in FITC and DAPI channels. Cardiomyocytic cross-sectional area (CSA) in 30–40 cells per animal was

manually determined using ImageJ (v1.54f). The assessor was blinded to the respective group.

2.8. Generation of RLN knockout mice

Sperm of RLN1 knockout mice (strain name C57BL/6N-Rln1 < tm1 (KOMP)Vlcg>/AB5) was obtained from the Experimental Animal Division of the RIKEN BioResource Research Center Japan. In-vitro fertilization was performed at the Interfaculty Biomedical Facility at the University of Heidelberg. Offspring were genotyped according to RIKEN protocol using ear biopsies obtained from 3-week-old offsprings.

2.9. Comparison to AAV9.huRXFP1 virus treated mice

A dosage of 1×10^{12} vg AAV9.huRXFP1 virus in a volume of 100 μl was injected into the tail vein of C57BL/6 mice and organs were
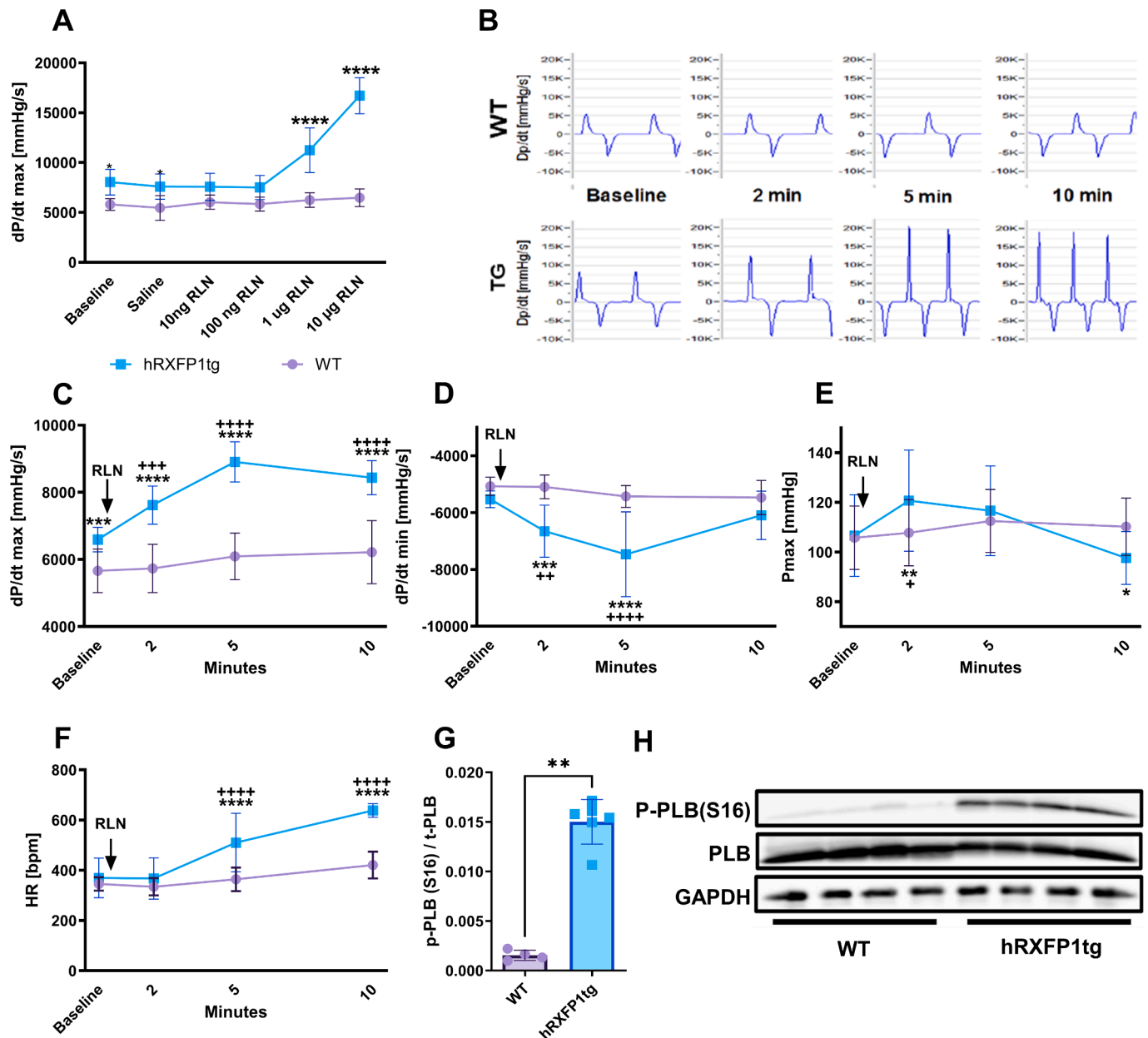
Fig. 2. RLN administration in hRXFP1tg mice results in positive inotropy. (A) Dose-response curve showing dP/dt maximum (dP/dt max) after injection of saline followed by increasing RLN concentrations between 10 ng and 10 μg in hRXFP1tg vs. WT mice. Baseline pressure loops were recorded for 10 min followed by recordings 4 min after each injection. n = 8 hRXFP1tg_high / 4 WT mice. (B-F) Baseline pressure loops were recorded for 10 min. hRXFP1tg vs. WT mice then received 10 μg RLN and pressure loops were recorded for another 15 min. n = 7 per group. (B) Representative pressure loop recordings; (C) dP/dt max; (D) dP/dt minimum (dP/dt min); (E) P maximum (Pmax); (F) Heart rate (HR). (G) Cardiac P-PLB(S16)/PLB quantification by immunoblot. (H) Representative immunoblot of P-PLB(S16)/PLB quantification. Glyceraldehyde-3-phosphate dehydrogenase (GAPDH) immunodetection was used as an internal control. Significant differences in (A)-(F) were determined by 2-way-ANOVA with repeated measures and Tukey's multiple comparisons test; * WT vs hRXFP1tg; + hRXFP1tg baseline vs timepoints; significance in (G) was determined by Mann-Whitney U test. Values represent the mean ± SD; * − p ≤ 0.05; ** − p ≤ 0.01; *** − p ≤ 0.001; **** − p ≤ 0.0001.

harvested 7 weeks after administration. Construction and production of recombinant vector stocks was performed as previously described [26].

2.10. TAC study design

The study results are reported in accordance with the ARRIVE (Animal Research: Reporting In Vivo Experiments) guidelines. Animals were randomized into respective groups, measurements and analysis were performed under blinded conditions. Cardiac function measurements were performed at day 0 before the respective operation (TAC- or sham-operation) and at day 7, day 28 and day 42. At day 45 animals were sacrificed, organs harvested and snap frozen for further analysis.

One TAC/hRXFP1tg_low animal (Fig. 4) died prior to echocardiography on day 28. No other animals were excluded. For Fig. 5, panels D-E and H-K, one RNA sample (hRXtg/RLNko Sham male) had to be excluded due to poor quality.

2.11. TAC operation

Anesthesia was induced by intraperitoneal (i.p.) injection. Either Ketamin (120 mg/kg body weight) (Ketamidor, WDT, Garbsen, Germany) and Xylazin (16 mg/kg body weight) (Xylavet, CP-Pharma, Burgdorf, Germany) (Fig. 3) or a combination of Medetomidin (500 μg/kg body weight) (Sedin, Vetpharma Animal Health, Barcelona,
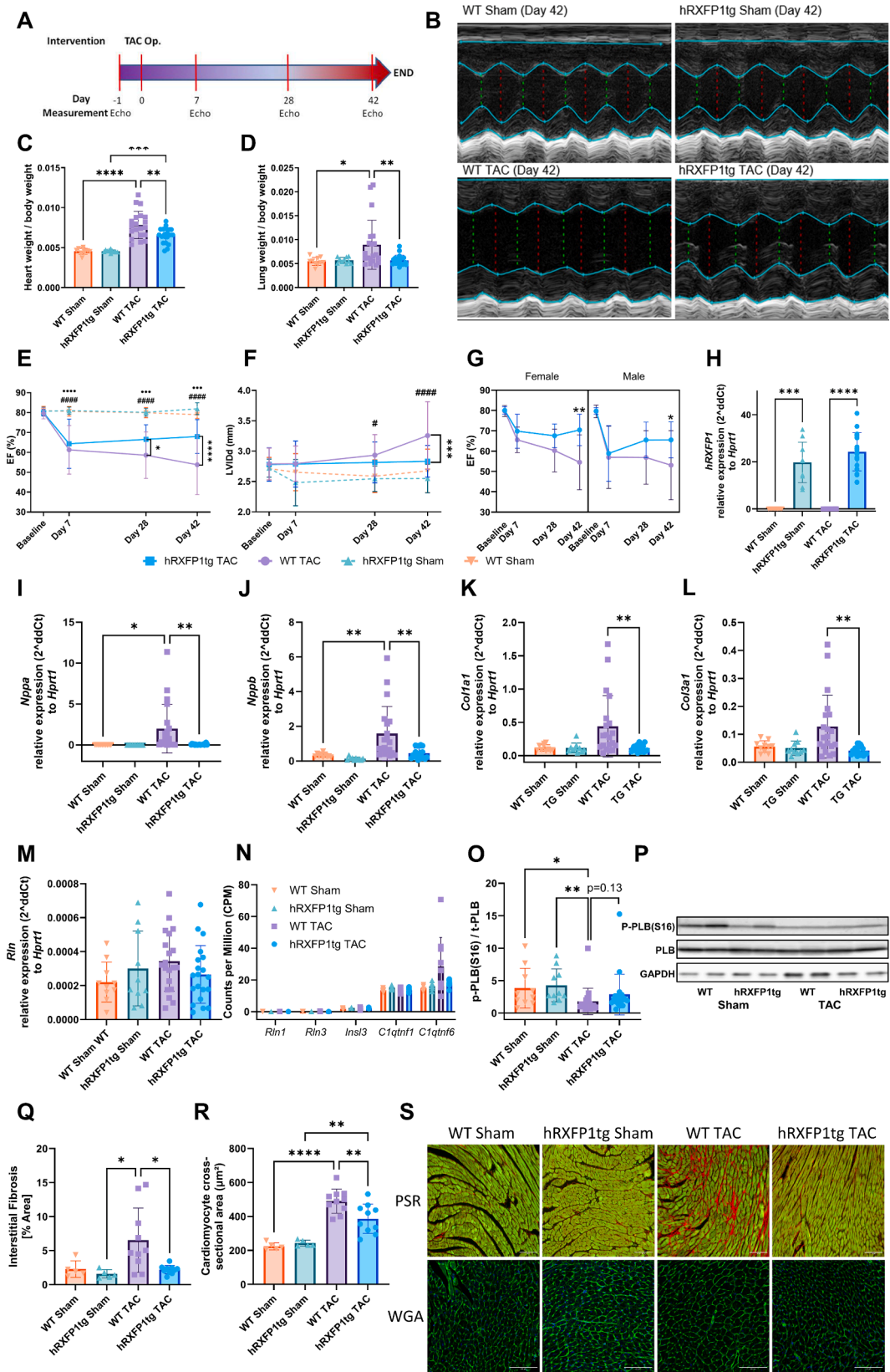
(caption on next page)

Fig. 3. hRXFP1tg are protected from TAC-induced cardiac dysfunction without additional RLN administration. hRXFP1tg_high and WT mice were randomized to Sham or TAC operation. (A)-(M) and (O)-(P) n = 20 per TAC-group, 10 per Sham-group. For (N) and (Q)-(S) only all male study animals were used. Each group comprised an equal distribution of female and male animals. (A) Experimental design. (B) Representative M−Mode echocardiogram recordings of experimental groups on day 42. (C) Heart weight to body weight ratios. (D) Lung weight to body weight ratios. (E)-(G) Echocardiographic measurements of (E) ejection fraction (EF); (F) left ventricular inner diastolic diameter (LVIDd); (G) ejection fraction by gender; * hRXFP1tg TAC vs. WT TAC; ●hRXFP1tg TAC vs. hRXFP1tg Sham; # WT TAC vs. WT Sham. (H)-(M) mRNA expression in the LV by qRT-PCR normalized to *Hprt1* of (H) hRXFP1tg; (I) *Nppa*; (J) *Nppb*; (K) Collagen 1A1 (*Col1a1*); (L) Collagen 3A1 (*Col3a1*); (M) *Rln*. (N) RNA-seq counts per million of *Rln1, Rln3, Insl3, C1qtnf1, C1qtnf6*. (O) Cardiac P-PLB(S16)/PLB quantification by immunoblot. (P) Representative immunoblot of P-PLB(S16)/PLB quantification. Glyceraldehyde-3-phosphate dehydrogenase (GAPDH) immunodetection was used as an internal control. (Q) Interstitial myocardial fibrosis and (R) cardiomyocyte cross-sectional area (CSA) quantified from histochemical staining with (S) representative Picrosirius Red (PSR) and Wheat Germ Agglutinin (WGA) staining images. Significant differences were determined by (C)-(D) and (Q)-(R) ordinary one-way ANOVA test with Tukey's multiple comparison test; (E)-(G) 2-way-ANOVA with repeated measures and Tukey's multiple comparisons test; (H)-(M) and (O) Kruskal-Wallis one-way ANOVA test with Dunn's multiple comparison test. Values represent the mean ± SD; *p < 0.05; **p < 0.01; ***p < 0.001; ****p < 0.0001.
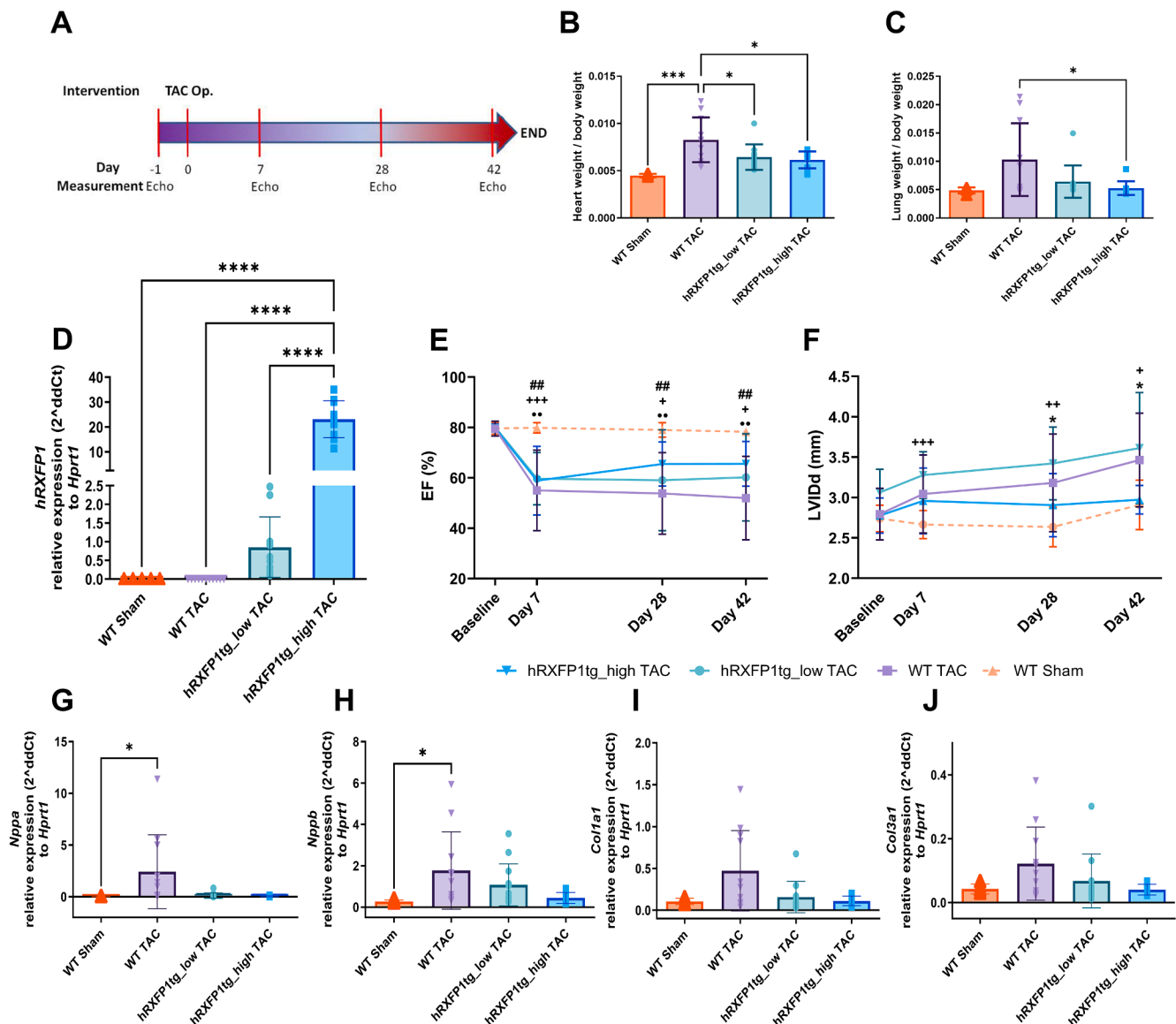
Fig. 4. Protective effects increase with higher hRXFP1tg expression. (A)-(J) Male hRXFP1tg mice with different transgene expression levels (hRXFP1tg_low vs. hRXFP1tg_high) and WT controls were randomized to Sham or TAC operation. n = 10 TAC/hRXFP1tg_high / 12 TAC/hRXFP1tg_low / 11 TAC/WT / 5 Sham/WT. 1 TAC/hRXFP1tg_low animal died before echocardiography on day 28 and was excluded from analysis. (A) Experimental design. (B) Heart weight to body weight ratios. (C) Lung weight to body weight ratios. (D) hRXFP1tg mRNA expression in the LV by qRT-PCR normalized to *Hprt1*. (E)-(F) Echocardiographic measurements of (E) ejection fraction (EF); (F) left ventricular inner diastolic diameter (LVIDd); ●hRXFP1tg_high TAC vs. WT Sham; # WT TAC vs. WT Sham; + hRXFP1tg_low TAC vs. WT Sham; *hRXFP1tg_low TAC vs. hRXFP1tg_high TAC. (G)-(J) mRNA expression in the LV by qRT-PCR normalized to *Hprt1* of (G) *Nppa*; (H) *Nppb*; (I) Collagen 1A1 (*Col1a1*); (J) Collagen 3A1 (*Col3a1*). Significant differences were determined by (B)-(C) ordinary one-way ANOVA test with Tukey's multiple comparison test; (D) and (G)-(J) Kruskal-Wallis one-way ANOVA test with Dunn's multiple comparison test; (E)-(F) 2-way-ANOVA with repeated measures and Tukey's multiple comparisons test. Values represent the mean ± SD. *p < 0.05; **p < 0.01; ***p < 0.001; ****p < 0.0001.

Spain), Midazolam (5 mg/kg body weight) (Dormicum, Roche, Mannheim, Germany) and Fentanyl (50 µg/kg body weight) (Hameln Pharma, Hameln, Germany) (Figs. 4-5) were used for anesthesia. Mice were intubated using a 22-gauge i.v. catheter. Ventilation was performed with a tidal volume of 200 µl, a respiratory rate of 150/min and 0.6 l/min oxygen flow. A blunt dissection of the aortic arch was performed through a partial thoracotomy in the first intercostal left space. The aortic arch was ligated in between the brachiocephalic and the left carotid arteries over a blunt 27-gauge needle using a 7.0 prolene suture. For sham mice, no ligation was performed. The incision was closed using a 6.0 prolene suture.

2.12. Echocardiography

Echocardiography was performed on wake animals using the Vevo 2100 Imaging System (FUJIFILM VisualSonics, Toronto, Canada). Using the linear ultrasound transducer MS400 (18–38 MHz), B-mode recordings of the left parasternal long and short axis view were obtained. Additionally, an M−mode recording of the LV at papillary muscle level was obtained from the short axis view. LV systolic function was quantified using the LV trace function of the Vevo Lab Software (FUJIFILM VisualSonics, Toronto, Kanada) on the M−mode recording (Fig. 3B).

2.13. Pressure-loop measurements

LV pressure measurements were obtained using the ADVantage system (type FY897B, Scisense, London, Canada). Anesthesia was performed using a combination of Medetomidin, Midazolam and Fentanyl as for TAC operation. The catheter tip was incubated in 37 °C saline solution for 30 min prior to measurement. Mice were placed on a heating plate in prone position; hair was removed from chest and neck and the neck area was disinfected. After incision and blunt dissection of the right carotid artery, the catheter tip was inserted in between two 6–0 prolene sutures and advanced into the LV. A baseline pressure curve was recorded for ten minutes. To establish dose–response curves, i.p. injections of saline followed by increasing concentrations of recombinant RLN were performed and pressure-loops were recorded 4 min after each injection. For time curve measurements, 10 µg of recombinant RLN were injected i.p., followed by another 10 min of pressure-loop recording. Measurements were performed on 30–40 consecutive pressure loops with LabScribe 4.3.

Besides maximal LV pressure (Pmax) and heart rate (HR), minimal and maximal rate of LV pressure change (dP/dt min, dP/dt max) as measures of LV relaxation and contractility were analyzed.

2.14. In-vivo receptor stimulation and analysis of phospholamban (PLB) phosphorylation

Mice received the same anesthesia as for pressure-loop measurements. Additionally, 10 mg/kg body weight Metoprolol (Lopresor, Novartis, Nuremberg, Germany) were applied to suppress effects of a systemic catecholamine release due to a stress response resulting from handling and injections on PLB phosphorylation. After 15 min, 10 µg recombinant RLN were injected i.p.. Heart tissue was harvested 5 min after RLN injection.

A 10–20 mg tissues piece was homogenized in 300 µl SDS lysis buffer (1 % [v/v] SDS (SERVA GmbH, Heidelberg, Germany), 1 mM EDTA (AppliChem GmbH, Darmstadt, Germany), 1 mM EGTA (SERVA GmbH, Heidelberg, Germany)) supplemented with Roche cOmplete protease inhibitor (Roche, Mannheim, Germany) and phosphatase inhibitor cocktails 2 and 3 (Sigma-Aldrich, Munich, Germany) using a bead mill. Cell debris was removed by centrifugation. After colorimetric measurement of protein concentrations, samples were diluted to 1–2 mg/ml, mixed with 6 µl 5xSDS loading buffer (30 % Glycerol (v/v) (AppliChem GmbH, Darmstadt, Germany), 50 mM TRIS (Carl-Roth, Karlsruhe, Germany), 10 % SDS (v/v) (SERVA GmbH, Heidelberg, Germany), 250 mM

DTT (Sigma Aldrich, Munich, Germany), 10 mM EDTA (AppliChem GmbH, Darmstadt, Germany), 0.1 % bromphenol blue (w/v) (Sigma Aldrich, Munich, Germany)) and separated on a 4–20 % Tris-Glycine gel (Thermo Fisher Scientific, Waltham, USA). Protein was transferred onto a PVDF blotting membrane (Immobilon-FL, Merck Millipore, Darmstadt, Germany) using a semi-dry transfer chamber. The membrane was incubated in blocking reagent (iBlock, Thermo Fisher Scientific, Waltham, USA) and probed with the following antibodies diluted in blocking reagent: PLB (mouse monoclonal; Thermo Fisher; Cat. MA3-922; dilution 1:5,000), P-PLB(S16) (rabbit polyclonal; Merck Millipore; Cat. 07–052; dilution 1:7,500), GAPDH (mouse monoclonal; Merck Millipore; Cat. MAB374; dilution 1:10,000) and anti-mouse secondary antibody coupled to Alexa Fluor 680 (Thermo Fisher Scientific; Cat. A-21057; dilution 1:10,000) and anti-rabbit secondary antibody coupled to Dylight 800 (Cell Signaling Technology; Cat. 5151; 1:10,000). Blots were washed in TBS-T (0.025 M Tris (Carl-Roth, Karlsruhe, Germany), 0.15 M NaCl (Carl-Roth, Karlsruhe, Germany), 1 mM CaCl2 (AppliChem GmbH, Darmstadt, Germany), 0.1 % Tween 20 (v/v) (Carl-Roth, Karlsruhe, Germany) and scanned using the Odyssey CLx imaging system (LI-COR Biosciences, Bad Homburg, Germany).

2.15. Tissue sample harvesting

Mice were sacrificed by cervical dislocation. Organs were removed. After washing in cold PBS (Sigma Aldrich, Munich, Germany) and removal of adherent tissue, the heart was weighed and cut into 9 pieces. Lungs were weighed. All tissues were frozen on dry ice and stored at −80 °C.

2.16. RNA isolation and quantitative real-time PCR (qRT-PCR)

A 10–20 mg tissues piece was added to 1 ml Trizol (Invitrogen, Karlsruhe, Germany) and homogenized using a bead mill. After adding 200 µl chloroform (Sigma Aldrich, Munich, Germany) the samples were shaken by hand and centrifuged. 400 µl of the transparent RNA-phase on top were removed into a new reaction vessel. After adding 400 µl isopropranolol (AppliChem, Darmstadt, Germany), the RNA was incubated overnight at −20 °C. Subsequently, the RNA was pelleted by centrifugation. The pellet was washed twice with 75 % ethanol (Sigma Aldrich, Munich, Germany), air-dried at room temperature, and resuspended in 20 µl DEPC-H$_2$O (Carl-Roth, Karlsruhe, Germany). Reverse transcription was performed using the iScript Reverse Transcription Supermix, qRT-PCR was performed using a Bio-Rad CFX96 real-time PCR detection system and SYBR Green PCR master mix (all Bio-Rad, Munich, Germany) according to manufacturer instructions. Relative gene expression levels were calculated using the 2ˆddCt method. qRT-PCR primers are listed in Table 1.

2.17. RNA-sequencing and bioinformatic analysis

Total RNA from LV cardiac tissue of 30 (5 wt Sham, 5 hRXFP1tg Sham, 10 wt TAC, 10 hRXFP1tg TAC) male animals were selected for RNA sequencing. RNA libraries were prepared for sequencing using standard BGISeq-500 protocols (Beijing Genomics Institute (BGI), Shenzhen, China). Strand specific RNA sequencing was performed on a DNBSEQ platform PE100bp in paired end mode. Reads were trimmed with trim_galore (v0.6.4) (available at https://github.com/FelixKrueger/TrimGalore), counts were created with TopHat (v2.1.1) [29] and bowtie (v2.2.9) [30,31], and counts per million (CPM) values were created using the cpm function of edgeR package (v3.17) [32–34]. edgeR was also used to calculate differential expression. Genes with a false discovery rate (FDR) < 0.05 and a log2-fold change (LogFC) > |1| were generally designated as differentially expressed between groups, except when stated otherwise. Volcano plots were created with ggVolcanoR [35]. Pathway Analysis was done using the IPA tool (QIAGEN Inc., https://www.qiagenbioinformatics.com/products/ingenuity-path
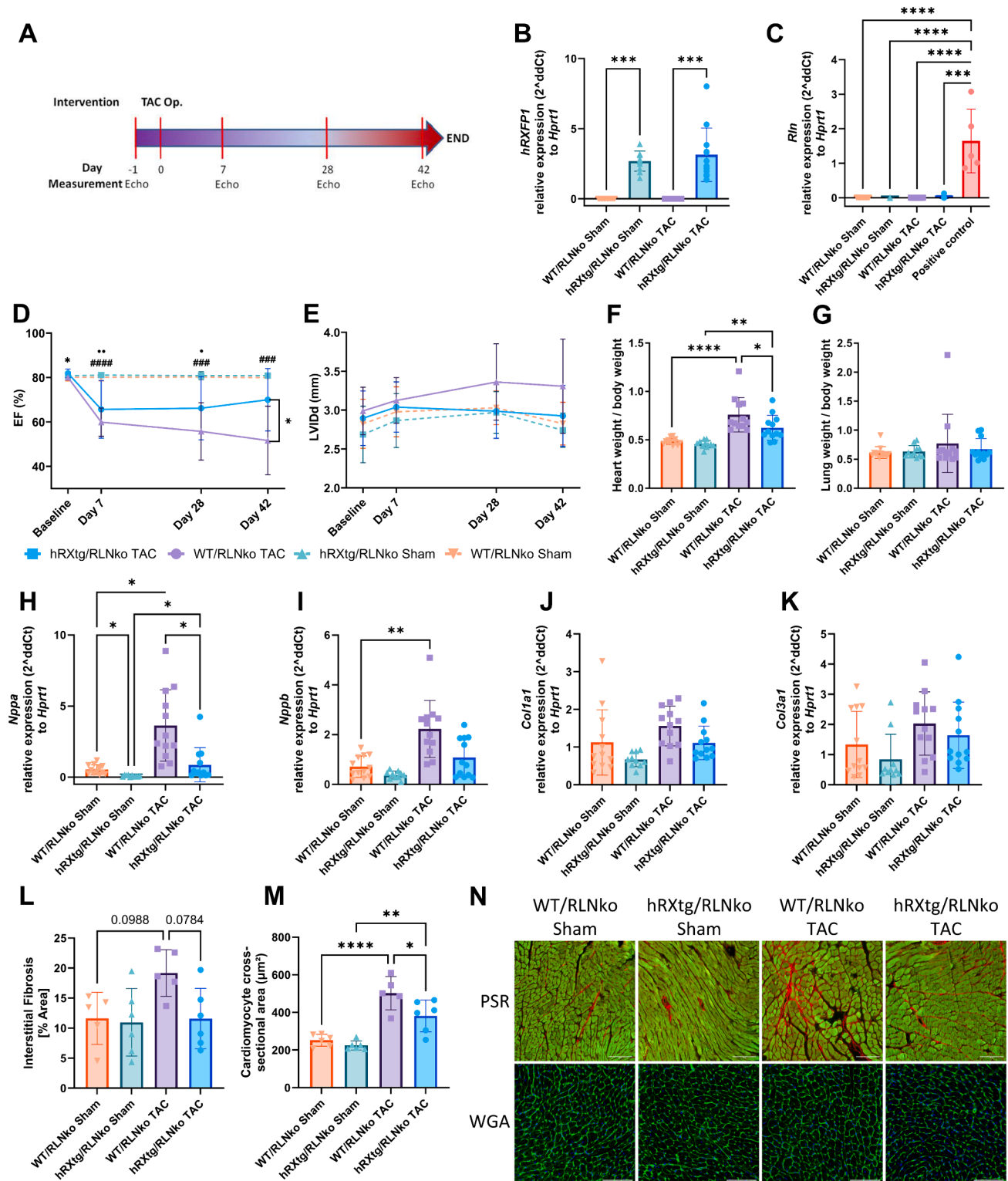
Fig. 5. Protective effects persist in the absence of systemic RLN. (A)-(K) RLN knockout mice with either hRXFP1tg_high (hRXtg/RLNko) or WT-RXFP1-expression (WT/RLNko) were randomized to Sham or TAC operation. n = 10–12 per group. Each group comprised an equal ratio of female and male animals. For (D-E and H-K), one sample (hRXtg/RLNko Sham male) had to be excluded due to poor RNA quality. For (L)-(N) only male study animals were used. (A) Experimental design. (B)-(C) mRNA expression of (B) hRXFP1tg and (C) RLN in the LV by qRT-PCR normalized to *Hprt1*. For (C), n = 5 mice with WT-RLN-expression were used as positive control. (D)-(E) Echocardiographic measurements of (D) ejection fraction (EF); (E) left ventricular inner diastolic diameter (LVIDd); * hRXFP1tg TAC vs. WT TAC; ●hRXtg/RLNko TAC vs. hRXtg/RLNko Sham; # WT/RLNko TAC vs. WT/RLNko Sham. (F) Heart weight to body weight ratios. (G) Lung weight to body weight ratios. (H)-(K) mRNA expression in the LV by qRT-PCR normalized to *Hprt1* of (H) *Nppa*; (I) *Nppb*; (J) Collagen 1A1 (*Col1a1*); (K) Collagen 3A1 (*Col3a1*). (L) Interstitial myocardial fibrosis and (M) cardiomyocyte cross-sectional area (CSA) quantified from histochemical staining with (N) representative Picrosirius Red (PSR) and Wheat Germ Agglutinin (WGA) staining images. Significant differences were determined by (B)-(C) and (H)-(K) Kruskal-Wallis one-way ANOVA test with Dunn's multiple comparison test; (D)-(E) 2-way-ANOVA with repeated measures and Tukey's multiple comparisons test; (F)-(G) and (L)-(M) ordinary one-way ANOVA test with Tukey's multiple comparison test. Values represent the mean ± SD. *$p < 0.05$; **$p < 0.01$; ***$p < 0.001$; ****$p < 0.0001$.

Table 1
PCR primers.

Gene	Application	Sequence	Annealing
Col1a1 Forward	qRT-PCR	GTGTTCCCTACTCAGCCGTC	57 °C
Col1a1 Reverse		ACTCGAACGGGAATCCATCG	
Col3a1 Forward	qRT-PCR	TGACTGTCCCACGTAAGCAC	57 °C
Col3a1 Reverse		GAGGGCCATAGCTGAACTGA	
Hprt1 Forward	qRT-PCR	GAGGAGTCCTGTTGATGTTGCCAG	55–65 °C
Hprt1 Reverse		GGCTGGCCTATAGGCTCATAGTGC	
hRXFP1 Forward	qRT-PCR	CTACAAGGACGACGATGACAAG	61 °C
hRXFP1 Reverse		GAAATAGCCAAGGGAGCACTTG	
hRXFP1 Forward	PCR (Genotyping)	CTACAAGGACGACGATGACAAG	63,5 °C
hRXFP1 Reverse		CTTCTGTGGACAGAATGGCCA	
hRXFP1 Forward	Sequencing	GGCACTTTACATGGAGTC	53,8 °C
hRXFP1 Mid		CAAGACTACATTGGCTGG	53,8 °C
hRXFP1 Reverse		CTGGAGTGGCAACTTCC	54,8 °C
Nppa Forward	qRT-PCR	TGCCGGTAGAAGATGAGGTC	63.5 °C
Nppa Reverse		TGCTTTTCAAGAGGGCAGAT	
Nppb Forward	qRT-PCR	CTGAAGGTGCTGTCCCAGAT	57 °C
Nppb Reverse		CCTTGGTCCTTCAAGAGCTG	
Rln Forward	qRT-PCR	GAGCCTTTCGATACGACGCT	59 °C
Rln Reverse		GCTGGCTCATCAATCCACCA	

way-analysis).

The raw data generated from this study are openly available at GEO (https://www.ncbi.nlm.nih.gov/geo/, GSE252607).

2.18. Chemicals

Recombinant RLN H2 was purchased from R&D Systems (Minneapolis, MN, USA). All chemicals were diluted and stored according to manufacturer's protocols.

2.19. Sample size determination

For all *in vivo* experiments, required sample sizes were determined a priori to ensure adequate power to detect statistically significant differences between groups. Power analysis for experiments with equal sample sizes was performed utilizing the R package pwr (v 1.3.0). With the aim of accommodating the 3R principles, the number of Sham animals was reduced where reasonable. To account for the resulting unequal sample sizes, a Monte Carlo Simulation (MG4C, v. 18.9.8) with random seeds and 10,000 iterations was performed for a priori as well as post hoc power analysis [36]. In any case, effect sizes were based on previous and published data, and a significance level of < 0.05 and a power of > 0.8 was desired.

Ejection Fraction (EF) served as primary outcome measure for the *in vivo* TAC studies due to the robustness of the parameter, whereas the study in Fig. 2 was powered for the difference in LV dP/dt max. For the study in Fig. 2, Cohen's d (for 10 min post inj.) was assumed as 1.6. 7 animals per group were necessary to ensure a power of 83 %, whereas post hoc analysis revealed that the achieved power was ∼ 99.9 %. For the group comparison WT/TAC vs. hRXFP1tg/TAC at 42 days post TAC

in Fig. 3, d = 1.2 was expected, and 20 animals in TAC or 10 in Sham groups, respectively, were necessary to ensure a power of > 85 % in a Tukey's mc test, whereas post hoc analysis revealed that the achieved power was 90 %. The results of Fig. 3 informed power analysis for Fig. 5. For the group comparison WT/RLNko/TAC vs. hRXtg/RLNko/TAC at 42 days post TAC, d = 1.4 was assumed, and 12 animals in each group were expected to ensure a power of > 85 % in a Tukey's mc test, whereas post hoc analysis, again, revealed that the achieved power exceeded 90 %. The TAC study in Fig. 4 as well as the data presented in Fig. 1 were planned as pilot studies, thus no a priori power calculation was performed.

2.20. Statistics and data presentation

Statistical analysis was performed using GraphPad Prism software version 10.1.2. Data are presented as means ± standard deviation (SD). To compare means among three or more independent groups with normal distribution, we performed one-way analysis of variance (ANOVA). A Tukey post hoc test was applied for multiple comparisons. For non-normal data distributions, a Kruskal-Wallis test was performed, and a Dunn's post hoc test was applied when multiple comparisons were conducted. Two-way ANOVA was used when appropriate. For all tests, a p value of < 0.05 was accepted as statistically significant. $*p < 0.05$; $**p < 0.01$; $***p < 0.001$; $****p < 0.0001$.

The graphical abstract was created using BioRender.com.

3. Results

3.1. Transgene expression, distribution, and phenotype in hRXFP1tg mice

Vector-based RXFP1 overexpression in combination with RLN supplementation could revert HF progression in a previous study. To examine the effects of isolated CM RXFP1 overexpression, transgenic mice (hRXFP1tg) were generated. For this purpose, the same cDNA-sequence of human RXFP1 carrying a n-terminal FLAG-tag was used [26]. The α-MHC promotor provides highly specific CM expression in the hRXFP1tg mice. Accordingly, hRXFP1 was mainly detectable in the myocardium of hRXFP1tg mice. Second highest level of hRXFP1 expression was the skeletal muscle. mRNA expression levels in other organs were negligible or below the detection limit (Fig. 1D).

Mice with 200 and 100 transgene copies per heterozygous genome were chosen as founders of the hRXFP1tg_high and hRXFP1tg_low lines. On mRNA level, either strain had significantly higher levels of hRXFP1 overexpression compared to AAV9.huRXFP1 virus treated mice. Mean cardiac hRXFP1 expression levels were 14-fold higher in the hRXFP1tg_low line and 227-fold higher in the hRXFP1tg_high line (Fig. 1B). hRXFP1 expression levels were equally distributed throughout the heart, with no significant differences between the atria and ventricles of the left and right heart (Fig. 1C). To facilitate detection of hRXFP1, an N-terminal FLAG-tag was added to the receptor. Using a monoclonal FLAG-antibody, IHC staining of hRXFP1 was achieved, with a visible staining along the cell membranes of transgenic CMs (Fig. 1F) beyond the background signal detectable in WT controls (Fig. 1E).

hRXFP1tg strains presented a phenotype similar to WT controls. In particular, no alterations with regard to the reproductive system or behavior were evident.

3.2. RLN administration in hRXFP1tg mice induces positive inotropy

To verify functionality of the transgenic RXFP1, pressure-loop recordings were performed in hRXFP1tg_high mice and WT controls.

Initially, we evaluated a dose range for RLN. In hRXFP1tg mice, there was a dose-dependent increase in dP/dt max (Fig. 2A), with significant differences observed compared to WT controls at RLN doses of 1 μg and 10 μg. Since maximum hemodynamic effects were attained at a dose of 10 μg, we selected this dose for subsequent time-curve experiments.

At baseline, a significantly increased dP/dt max was detected in hRXFP1tg mice (Fig. 2C). There were no baseline differences concerning dP/dt min (Fig. 2D), Pmax (Fig. 2E) or HR (Fig. 2F). I.p. RLN injection induced a significant rise in dP/dt max at 2 min, reaching a peak at 5 min (Fig. 2C). In parallel dP/dt min decreased in a reciprocate manner (Fig. 2D) in hRXFP1tg mice. Positive inotropy resulted in an initial increase of Pmax in hRXFP1tg mice with a significantly higher Pmax compared to WT at 2 min after RLN injection. Subsequently, Pmax decreased below baseline values. At 10 min after RLN injection Pmax was significantly lower in hRXFP1tg compared to WT (Fig. 2E). Secondary to the decrease in Pmax, hRXFP1tg mice showed a significant upsurge in HR (Fig. 2F). In contrast, WT mice did not react with any significant changes in either parameter (Fig. 2B-2F). In line with the previously proposed signaling pathway for RXFP1/RLN signaling in CM and the observed increase in contractility, a significant increase in P-PLB (S16)/PLB ratio could be detected in hRXFP1tg animals (Fig. 2G-H).

3.3. hRXFP1tg are protected from TAC-induced cardiac dysfunction

Effects of CM specific hRXFP1 overexpression were evaluated in the TAC-model of pressure-overload induced HF. hRXFP1tg_high and WT mice were randomized to Sham or TAC operation and underwent regular echocardiographic examinations until sacrifice at day 45 (Fig. 3A). Each group comprised an equal distribution of female and male animals. Pressure overload induced cardiac hypertrophy resulting in significantly increased heart to body weight ratios (HW/BW) in both TAC-operated groups (Fig. 3C). However, hRXFP1tg showed significantly less cardiac hypertrophy after TAC compared to WT controls (Fig. 3C). Lung weight to body weight ratios (LW/BW) as a readout of pulmonary congestion were significantly attenuated in hRXFP1tg. While TAC/WT animals showed a significant rise in LW/BW, TAC/hRXFP1tg mice did not present with significant pulmonary congestion (Fig. 3D). On echo, EF decreased in all TAC-operated animals until day 7 (Fig. 3E). However, TAC/hRXFP1tg showed a significant recovery of EF in the further course of the study, whereas TAC/WT animals presented a progressive decline in EF. This resulted in a significantly improved EF in TAC/hRXFP1tg compared to TAC/WT at day 28 and 42 (Fig. 3E). This held true for both male and female mice (Fig. 3G). Pronounced diastolic LV inner diameter (LVIDd) dilation, a hallmark of progressive HF, was evident in TAC/WT animals. This was abrogated in TAC/hRXFP1tg mice (Fig. 3F). Analysis of ventricular mRNA expression confirmed significant levels of hRXFP1 mRNA in transgenic animals (Fig. 3H). *Nppa* and *Nppb* mRNA expression was significantly higher in TAC/WT compared to Sham/WT animals, whereas no significant increase in *Nppa* and *Nppb* levels was detectable in TAC/hRXFPtg animals (Fig. 3I-3J). In line with these observations, significantly lower expression levels of fibrotic marker genes Collagen-1 (*Col1a1*) and -3 (*Col3a1*) were measured in TAC/hRXFP1tg compared to TAC/WT animals (Fig. 3K-3L). Conversely, the ratio of P-PLB(S16)/PLB significantly decreased only in TAC/WT mice, not in TAC/hRXFP1tg mice (Fig. 3O-3P). Low levels of RLN mRNA expression in the LV were detectable in all groups, with no significant differences due to genotype or treatment (Fig. 3M). The same applied for RNA-seq expression levels of the potential RXFP1 ligands *Rln3, Insl3 and Ctqtnf1* (Fig. 3N). Only *Ctqtnf6* expression was increased in TAC/WT animals while TAC/hRXFP1tg presented expression levels similar to Sham (Fig. 3N).

In histochemical staining, TAC induced interstitial fibrosis and significant CM hypertrophy (Fig. 3Q-3S). However, fibrosis (Fig. 3Q) and CM hypertrophy (Fig. 3R) were significantly attenuated in hRXFP1tg after TAC compared to WT controls.

These results indicate that overexpression of hRXFP1tg alone is adequate to mitigate cardiac dysfunction and remodeling, even without additional RLN administration.

3.4. Cardioprotection correlates with hRXFP1tg expression levels

Male hRXFP1tg mice with different transgene expression levels

(hRXFP1tg_low vs. hRXFP1tg_high) underwent TAC-operation and follow-up according to the earlier TAC-study (Fig. 4A). hRXFP1tg_high animals showed significantly higher levels of hRXFP1 in the LV compared to hRXFP1tg_low mice (Fig. 4D). HW/BW and LW/BW ratios were highest in the TAC/WT group, slightly lower in the hRXFP1tg_low group and significantly reduced in the hRXFP1tg_high group (Fig. 4B-4C), suggesting dose-dependent protective effects of CM-specific hRXFP1 expression. A similar dose-dependency was detectable for systolic LV function (EF, Fig. 4E) and ventricular geometry (LVIDd, Fig. 4F). However, progressive LV dilation was only fully abrogated in hRXFP1tg_high animals, while hRXFP1tg_low mice underwent LV dilation despite maintained systolic LV function.

In accordance with these findings, mRNA expression of natriuretic peptides *Nppa* and *Nppb* (Fig. 4G-4H) and remodeling markers *Col1a1* and *Col3a1* (Fig. 4I-4J) remained at Sham levels with yet numerically higher values in hRXFP1tg_low compared to hRXFP1tg_high mice.

3.5. RXFP1 protective effects persist in the absence of RLN

To examine whether CM-specific hRXFP1 overexpression is beneficial in the absence of systemic RLN, hRXFP1tg_high (hRXtg) mice were cross bred with RLN knockout mice (RLNko) to obtain hRXtg/RLNko. hRXtg/RLNko mice and WT/RLNko mice were then again subjected to TAC (Fig. 5A). Correct genotype and efficient RLN knockout were confirmed on mRNA level (Fig. 5B-5C).

Following an initial decline in EF after TAC, EF gradually improved in hRXtg/RLNko, whereas WT/RLNko mice presented a progressive decline in EF (Fig. 5D). Accordingly, hRXtg/RLNko mice were protected from LV dilation after TAC (Fig. 5E). At study end, hRXtg/RLNko mice revealed a significantly lower HW/BW ratio and a numerically lower LW/BW ratio compared to WT/RLNko mice (Fig. 5F-5G) indicating reduced cardiac hypertrophy and pulmonary congestion. In line with these observations, TAC/hRXtg/RLNko mice showed significantly lower *Nppa* expression levels than TAC/WT/RLNko mice (Fig. 5H), a similar trend was detectable concerning *Nppb* (Fig. 5I), *Col1a1* (Fig. 5J) and *Col3a1* (Fig. 5H).

Sham/hRXtg/RLNko exhibited significantly diminished *Nppa* values compared to Sham/WT/RLNko (Fig. 5H). A similar trend was detectable concerning *Nppb* (Fig. 5I), *Col1a1* (Fig. 5J) and *Col3a1* (Fig. 5H), suggesting baseline cardioprotective effects of hRXFP1tg in RLNko mice.

In histochemical staining, TAC induced significant CM hypertrophy in TAC-operated animals (Fig. 5M). However, CM hypertrophy (Fig. 5M) was significantly abrogated in hRXtg/RLNko after TAC compared to WT/RLNko controls. A similar trend was detectable concerning interstitial fibrosis (Fig. 5L). In general, levels of interstitial fibrosis were much higher in RLNko mice (Fig. 5L) compared to mice with WT RLN expression (Fig. 3Q).

These results indicate that CM-specific hRXFP1 overexpression can attenuate cardiac dysfunction and cardiac remodeling even in the absence of systemic RLN.

3.6. Transgenic RXPF1 expression reverts typical HF gene expression profiles

We performed RNA-seq from LV tissue of male WT Sham, WT TAC, hRXFP1tg_high Sham, and hRXFP1tg_high TAC mice to decipher potential signaling pathways modulated by hRXFP1.

In WT mice, TAC operation induced a significant response in gene expression with 2236 differentially regulated genes (DEG). Of these, 1321 were up- and 1100 downregulated, respectively (Fig. 6A). In contrast, merely 162 and 93 genes were found to be significantly up- or down-regulated in hRXFP1tg following TAC. Of these, only a small portion (39 and 31) were uniquely regulated in hRXFP1tg animals (Fig. 6B). A total of 33 genes were found to be uniquely regulated between WT Sham and hRXFP1tg_high Sham mice while we detected 594 up- and 969 down-regulated genes in TAC-operated hRXFP1tg animals
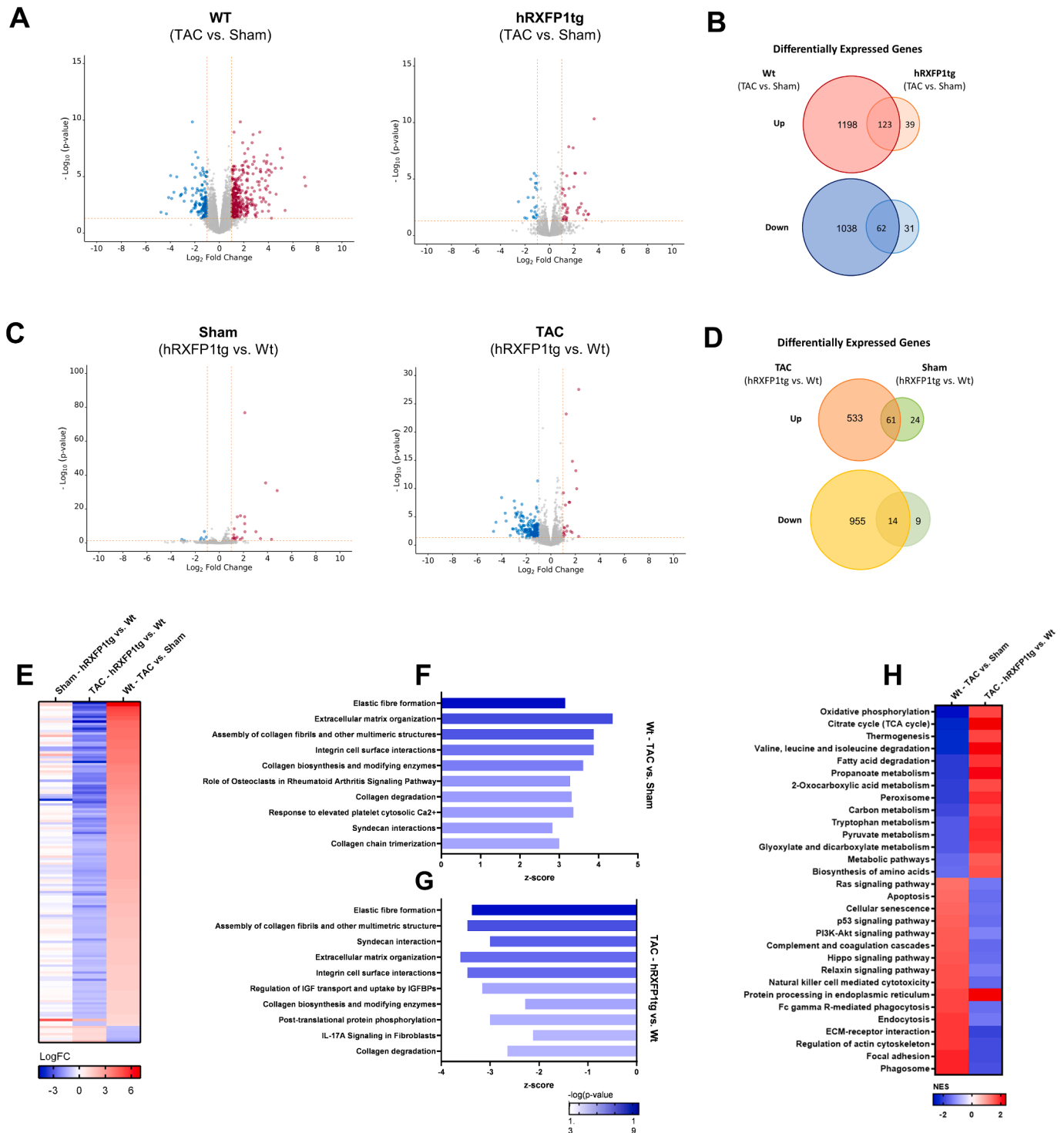
Fig. 6. Bulk RNAseq analysis reveals a normalized cardiac phenotype and energy metabolism in hRXFP1tg mice. (A)-(H) Total RNA from LV cardiac tissue of 30 (5 wt Sham, 5 hRXFP1tg Sham, 10 wt TAC, 10 hRXFP1tg TAC) male animals were selected for RNA sequencing. (A) Volcano plots of differentially expressed genes (DEGs) in TAC compared to Sham mice with the indicated genetic background. Horizontal yellow lines denote the false discovery rate (FDR) cutoff (FDR < 0.05), vertical yellow lines denote the Log Fold Change (LogFC) cutoff (LogFC > |1|). DEGs are color-coded, with blue indicating down-regulated (LogFC < -1), red indicating up-regulated (LogFC > 1), and grey dots indicating essentially non-regulated DEGs (LogFC < |1|). (B) Venn diagram showing overlapping up (top) and down-regulated (bottom) DEGs (FDR < 0.05) in the indicated groups. (C) Volcano plots of DEGs in hRXFP1tg compared to WT mice with the indicated treatment. Horizontal yellow lines: FDR < 0.05, vertical yellow lines: LogFC > |1|. (D) Venn diagram showing overlapping up (top) and down-regulated (bottom) DEGs (FDR < 0.05) in the indicated groups. (E) DEGs in Sham-treated hRXFP1tg vs. WT mice (column 1), TAC-treated hRXFP1tg vs. WT mice (column 2), and TAC vs. Sham-treated WT mice (column 3). DEGs with FDR < 0.05 and LogFC > |1| in groups of columns 2 and 3. (F-G) Ingenuity Pathway Analysis of DEGs in (F) TAC vs. Sham-treated WT and (G) TAC-treated hRXFP1tg vs. WT mice. The graph shows the z-score of the 10 top significantly enriched terms, whereas the shade of each bar represents the associated −log(p-value). (H) Heat map of top 15 significantly (FDR < 0.05) up- and down-regulated KEGG pathways in TAC vs. Sham-treated WT (column 1) and TAC-treated hRXFP1tg vs. WT (column 2) mice.

when compared to WT animals (Fig. 6C-6D).

The top TAC induced DEGs (Fig. 6E) were then used for Ingenuity Pathway Analysis (IPA). TAC primarily induced pathways related to fibrosis (such as elastic fiber formation, extracellular matrix organization, and assembly of collagen fibrils) compared to Sham-operated WT animals (Fig. 6F).

Most pathways identified by IPA in WT mice were found to be downregulated in TAC-operated hRXFP1tg. Again, fibrotic pathways, including the Syndecan interaction pathway, were ranking among the top 10 enriched pathways (Fig. 6G).

KEGG pathway analysis detected significant downregulation of cellular metabolism in WT mice upon TAC, a known adaption in HF. Among the top 15 activated pathways, hypoxic, pro-fibrotic, catabolic, and apoptotic pathways were found (Fig. 6H).

Comparing TAC-operated hRXFP1tg mice to their WT counterparts, the activation profile was largely reversed, except for the protein processing in endoplasmic reticulum pathway, potentially induced by the transgene itself.

These data reveal a mostly normalized gene expression in RXFP1tg mice compared to WT. Specifically, pro-fibrotic activity was found to be mitigated by RXFP1 while a physiological metabolic profile is maintained.

4. Discussion

In a previous study, vector-based RXFP1 overexpression in CMs combined with RLN administration was able to restore LV systolic function and to reduce pathological remodeling in mice upon TAC [26]. However, there were no clear indications of significant differences in typical RLN signaling aspects, such as fibrosis attenuation [26]. Yet, even without additional RLN administration, vector-based RXFP1 overexpression showed a trend towards attenuated HF development [26]. Considering these observations, we sought to assess whether isolated RXFP1 overexpression alone could suffice to attenuate HF, the potential role of endogenous RLN in this scenario, and its impact on fibrosis.

To facilitate assessment of therapeutic hRXFP1 properties at expression levels higher than achieved by our previous vector delivery, hRXFP1 transgenic mice (hRXFP1tg) with distinct expression intensities were generated. These mice are expressing the same cDNA-sequence of human FLAG-tagged RXFP1 as delivered by our AAV [26]. However, in the hRXFP1tg, expression is driven by the α-MHC promotor. Compared to the truncated MHC2v promotor used for vector delivery, α-MHC is highly specific for CMs and pulmonary vasculature, with low expression in skeletal muscle and no relevant expression in other tissues [37]. Accordingly, we found homogenous RXFP1 expression in all parts of the heart. Expression levels in skeletal muscle were less than 16 % and expression in other tissues was negligible. While fibroblasts have been reported to exhibit minimal activity of α-MHC promotors [37], the possibility of low levels of hRXFP1 expression in cardiac fibroblasts cannot be fully excluded in this context. There was no clinically apparent basal phenotype in hRXFP1tg mice detectable.

Proper transgene expression was confirmed by IHC detection of the receptor via the n-terminal FLAG-tag. We found robust CM staining beyond the unspecific background signal observed in WT controls. RXFP1 expression was predominantly located at the CM plasma membrane implying proper intracellular receptor trafficking. RLN is known to induce positive inotropy in atrial CMs with endogenous RXFP1 expression [20]. Thus, *in vivo* coupling of the hRXFP1 was assessed by hemodynamics. As anticipated, i.p. RLN injection induced a significant inotropic response in hRXFP1tg mice. Of note, a significant rise in contractility preceded any chronotropic response and was already detectable at 2-min post RLN. At this timepoint HR remained at baseline levels. The subsequent rise in HR in hRXFP1tg at 5- and 10-min post RLN can be attributed to both the chronotropic RLN effects [2,38] and the parallel decline in systolic pressure (Pmax). Upon RLN injection, Pmax

started to rise within the first 2 min before declining below baseline. The decline in Pmax while contractility was still rising suggests direct RLN effects on the vasculature. RLN is known to decrease systemic vascular resistance, resulting in a modest decrease in Pmax after *in vivo* infusion [2,38]. However, the absence of Pmax effects in WT controls indicates a transgene-dependent mechanism. Hemodynamically, this could be attributable to a mismatch of increased cardiac output and disposable preload, where the latter is disturbed by anesthesia and invasive ventilation.

On the molecular level, we found a rise in PLB(S16) phosphorylation, a well-established link to positive inotropy through RXFP1/protein kinase A (PKA) signaling [39]. Yet, detection requires suppression of β-adrenergic (β-AR) signaling as transportation and handling of mice prior to tissue collection cause sufficient catecholamine release to conceal RLN/RXFP1 specific PLB phosphorylation. This is supported by our previous data comparing β-AR and RXFP1 induced cyclic adenosine monophosphate (cAMP) responses [26]. Notably, hRXFP1tg presented increased contractility compared to control animals even prior to RLN injection. This supports the notion that RXFP1 signaling in CM occurs without the need for additional RLN administration.

To assess whether RLN supplementation is required to exploit RXFP1-cardioprotection, hRXFP1tg mice were subjected to pressure-overload by TAC. Transgenic mice presented not only an attenuated decline in LV function but even a gradual recovery of systolic function. At very high hRXFP1 expression levels even LV-dilation and thus progression to overt HF was abrogated.

Molecularly, transgenic hearts had significantly less activation of the fetal gene program as well as lower expression levels of fibrosis markers. This transfers to a significant mitigation of fibrosis and CM hypertrophy in myocardial sections. In accordance, transcriptomic profiling of TAC-operated hRXFP1tg mice revealed only discrete pro-fibrotic regulation as well as an improved metabolic profile. This implies a globally normalized transcriptomic profile in hRXFP1tg, providing robust evidence for the significant therapeutic potential of RXFP1 signaling. Thus, elevated RXFP1 expression levels in CMs without supplementary RLN administration seem to yield similar cardioprotective effects as vector-based RXFP1 overexpression combined with RLN administration [26]. These protective effects were evident in both sexes.

These observations raised the question if *in vivo* hRXFP1-signaling requires RLN. Due to a conserved region of 12 amino acids [40], the murine counterpart to H2 RLN, M1 RLN, also binds to hRXFP1 with high affinity and vice versa [41]. Consequently, circulating M1 RLN could activate hRXFP1. In mice, circulating RLN is mainly detectable during the menstrual cycle and pregnancy, when it exhibits its endocrine functions [38]. However, hRXFP1tg were protected from TAC independently of sex and outside of pregnancy. For RLN-knockout mice an age-related fibrosis of lung, heart, and kidneys with associated organ dysfunction has been described [16], suggesting autocrine or paracrine functions of RLN apart from pregnancy. This assumption is supported by reports of RLN expression outside the reproductive tract, in organs like thymus, kidney, and heart [38]. Detection of circulating murine RLN at protein level was not successful due to limited sensitivity of available ELISA kits. However, the concomitant peak of serum RLN levels [42] and placental and decidual RLN gene expression [43] during gestation suggests a robust correlation between mRNA levels and the amount of protein. This notion is further supported by a congruent upregulation in myocardial mRNA expression and circulating RLN in human HF trials [44]. Consistently, we detected low levels of RLN mRNA expression in the murine LV independent of genotype and gender. However, neither RXFP1 overexpression nor TAC induced significant alterations in RLN expression in our mice. This is certainly controversial, given the mentioned upregulation in human HF [44]. Yet, this could be attributable to species differences but also distinct severity of HF in the respective observations. Overall, regulation of RLN expression in myocardium will require further investigation including different HF animal models.

To assess the role of endogenous RLN in this context, hRXtg/RLNko mice were generated. Surprisingly, we found persisting protective effects following TAC, indicating a mechanism of hRXFP1 signaling independent of RLN. hRXtg/RLNko reacted similar to pressure-overload as hRXFP1tg mice, with an initial decay in EF followed by a gradual recovery, while WT/RLNko mice revealed a progressive deterioration. Activation of fetal genes and CM hypertrophy were again abrogated, while fibrotic markers and interstitial fibrosis were not significantly mitigated. The latter can be attributed to the higher baseline fibrosis in RLNko mice and lower n-number in this cohort. Additionally, we observed baseline cardioprotective effects in hRXtg/RLNko mice. These observations are in line with previous findings, reporting increased ventricular collagen in male RLN-knockout mice with resulting chamber stiffness and diastolic dysfunction [45]. This supports the notion that the absence of endogenous RLN by itself is a pathological stimulus abrogated by hRXFP1tg.

For RXFP1, distinctive signaling modalities depending on presence and concentration of stimulating RLN are described. Nanomolar RLN stimulation leads to G-protein coupling with stimulation of adenylyl cyclase (AC) resulting in intracellular cAMP accumulation [46]. In the absence of any ligand, RXFP1 forms a constitutively active signalosome resulting in a basal cAMP production by AC2, which can be activated by subpicomolar concentrations of RLN, whereas higher concentrations of RLN lead to dissociation of the signalosome [47]. Even though intrinsic constitutive activity and classic G-protein coupling both result in cAMP production, the different mechanisms of receptor activation result in specific cAMP pools with distinct cellular responses [46,47]. Yet, the therapeutic effects observed in vector-based RXFP1 overexpression and supra-nanomolar RLN supplementation [26] did not substantially differ from those observed in hRXFP1tg nor hRXtg/RLNko. This might serve as an argument against intrinsic receptor activity causing observed hRXFP1tg effects, however, it cannot be excluded at this point.

As another option, RXFP1 heterodimerization could explain effects of hRXFP1tg in the absence of endogenous RLN. RXFP1 heterodimerization is described with RXFP2 [48], Angiotensin II type 2 receptor (AT2R) [49] and Angiotensin II type 1 receptor (AT1R) [50]. As RXFP2 expression is not described in human or murine hearts [38], it is unlikely to interact with hRXFP1. AT1R and AT2R, however, are abundantly expressed in heart tissue and both form constitutive heterodimers with RXFP1 independent of ligand binding [49,50]. RXFP1-AT2R and RXFP1-AT1R heterodimerization has been shown by BRET experiments in HEK293-cells expressing RXFP1 [49,50], there is evidence of AT1R-AT2R-RXFP1 crosstalk *in vitro* in rat renal myofibroblasts [50] and human primary cardiac myofibroblasts [50,51] as well as *in vivo* in a murine model of kidney fibrosis and a model of isoproterenol (ISO)-induced cardiomyopathy [50]. Even though there is no concrete evidence concerning AT1R-AT2R-RXFP1 crosstalk in CMs as of now, concurrent expression in CMs makes AT1R-AT2R-RXFP1 crosstalk a possible explanation for hRXFP1tg effects independent of ligand binding.

Finally, hRXFP1tg could have been activated by another ligand than M1 RLN. In mice, known ligands of RXFP1 comprise insulin-like peptide 3 (INSL3) [52,53] and M3 RLN [54,55]. While INSL3 interacts with RXFP1 only at supraphysiological concentrations *in vitro* [52,53], H3 RLN has been demonstrated to be a lower potency activator of RXFP1 *in vitro* (30-fold less potent than H2 RLN) [56] and *in vivo* [57]. However, endogenous expression of M3 RLN was not sufficient to protect M1 RLN knockout mice from developing an age-related organ fibrosis [45,58], suggesting a limited potency of potential cardioprotective effects.

Suspected murine ligands of RXFP1 warranting further investigation include complement C1q tumor necrosis factor-related proteins (CTRPs) CTRP1 and CTRP6 [59,60], whereas CTRP8, a known RXFP1-ligand in humans [61], is not expressed in mice [62]. While expression levels of potential RXFP1 ligands M3 RLN, INSL 3 and CTRP1 presented no significant differences due to genotype or treatment, CTRP6 was elevated in TAC/WT mice but not increased in TAC/hRXFP1tg. CTRP6 is known

to mediate anti-fibrotic effects in the cardiovascular system [63] and to be upregulated in response to TAC [64]. Therefore, normalized CTRP6 gene expression levels in TAC/hRXFP1tg mice are in line with the globally normalized transcriptomic profile in hRXFP1tg.

Molecularly, we could confirm RLN induced PLB(S16) phosphorylation in hRXFP1tg mice and we detected a trend towards preserved PLB (S16) phosphorylation in TAC-operated hRXFP1tg. PLB-phosphorylation is known to be decreased in HF [65] and a well-established link to positive inotropy through RXFP1 signaling [39]. Therefore, RXFP1-PKA-PLB remains the most probable pathway for mediating positive inotropy in hRXFP1tg TAC mice. However, our current observations imply further research on RXFP1 downstream signaling in CM.

Limitations and future perspectives:

This study underscores the therapeutic potential of RXFP1, which persists regardless of endogenous RLN expression. RXFP1 mitigated remodeling, while RLN supplementation induced robust inotropy in RXFP1-overexpressing myocardium. However, there are limitations to this study: (1) Confirmation of RLN knockout was confined to the expression level, as protein detection, particularly of circulating RLN, was not reliably feasible. (2) In vivo hemodynamics were solely assessed at the highest stimulation level (10 μg), potentially limiting our understanding of the dose–response relationship and the comprehensive hemodynamic effects of RLN across various dosage levels. (3) While our findings demonstrated significant attenuation of remodeling, establishing causality remains challenging. It is plausible that the observed effects could be secondary to overall increased contractility rather than a direct consequence of RXFP1 overexpression. Further investigations are warranted to elucidate the precise mechanisms underlying these observed effects and to ascertain the causal relationship between RXFP1 expression and attenuated cardiac remodeling.

We envision vector-based RXFP1 overexpression in CM along with RLN administration as a therapeutic approach for patients with chronic HF and recurrent congestion. Here, we provide evidence on safety of RXFP1 at high overexpression levels and underline the protective potential of RXFP1, which protects from TAC-induced cardiac dysfunction even without additional RLN administration. These discoveries may lay the groundwork for an enhanced translational strategy, wherein RXFP1 overexpression offers foundational protection, complemented by selective RLN supplementation for targeted activation when needed. Nevertheless, additional investigation into appropriate RLN dosages, the mechanisms of RXFP1 activation, and its downstream effects in CMs is necessary to support ongoing translational endeavors.

CRediT authorship contribution statement

J. Wingert: Writing – review & editing, Writing – original draft, Visualization, Methodology, Investigation, Formal analysis, Conceptualization. **E. Meinhardt:** Writing – review & editing, Writing – original draft, Visualization, Supervision, Methodology, Investigation, Formal analysis, Conceptualization. **N. Sasipong:** Methodology, Formal analysis, Investigation, Supervision. **M. Pott:** Methodology, Investigation, Formal analysis. **C. Lederer:** Methodology, Investigation, Formal analysis. **C. de la Torre:** Methodology, Formal analysis, Investigation. **C. Sticht:** Software, Methodology, Investigation, Formal analysis. **P. Most:** Supervision, Resources, Conceptualization. **H.A. Katus:** Supervision, Resources, Funding acquisition, Conceptualization. **N. Frey:** Supervision, Resources, Funding acquisition, Conceptualization. **P.W.J. Raake:** Supervision, Resources, Methodology, Funding acquisition, Conceptualization. **P. Schlegel:** Writing – review & editing, Writing – original draft, Supervision, Project administration, Methodology, Investigation, Funding acquisition, Conceptualization.

Declaration of competing interest

The authors declare the following financial interests/personal

References

[1] G. Savarese, P.M. Becher, L.H. Lund, P. Seferovic, G.M.C. Rosano, A.J.S. Coats, Global burden of heart failure: a comprehensive and updated review of epidemiology, Cardiovasc. Res. 118 (17) (2023) 3272–3287.

[2] M. Sarwar, X.J. Du, T.B. Dschietzig, R.J. Summers, The actions of relaxin on the human cardiovascular system, Br. J. Pharmacol. 174 (10) (2017) 933–949.

[3] J.T. McGuane, J.E. Debrah, L. Sautina, Y.P. Jarajapu, J. Novak, J.P. Rubin, M.B. Grant, M. Segal, K.P. Conrad, Relaxin induces rapid dilation of rodent small renal and human subcutaneous arteries via PI3 kinase and nitric oxide, Endocrinology 152 (7) (2011) 2786–2796.

[4] D.O. Debrah, K.P. Conrad, A. Jeyabalan, L.A. Danielson, S.G. Shroff, Relaxin increases cardiac output and reduces systemic arterial load in hypertensive rats, Hypertension 46 (4) (2005) 745–750.

[5] Q. Xu, A. Chakravorty, R.A. Bathgate, A.M. Dart, X.J. Du, Relaxin therapy reverses large artery remodeling and improves arterial compliance in senescent spontaneously hypertensive rats, Hypertension 55 (5) (2010) 1260–1266.

[6] C.S. Samuel, E.N. Unemori, I. Mookerjee, R.A. Bathgate, S.L. Layfield, J. Mak, G.W. Tregear, X.J. Du, Relaxin modulates cardiac fibroblast proliferation, differentiation, and collagen production and reverses cardiac fibrosis in vivo, Endocrinology 145 (9) (2004) 4125–4133.

[7] J. Zhang, Y.F. Qi, B. Geng, C.S. Pan, J. Zhao, L. Chen, J. Yang, J.K. Chang, C.S. Tang, Effect of relaxin on myocardial ischemia injury induced by isoproterenol, Peptides 26 (9) (2005) 1632–1639.

[8] C.S. Samuel, H. Bodaragama, J.Y. Chew, R.E. Widdop, S.G. Royce, T.D. Hewitson, Serelaxin is a more efficacious antifibrotic than enalapril in an experimental model of heart disease, Hypertension 64 (2) (2014) 315–322.

[9] C.S. Samuel, S. Cendrawan, X.M. Gao, Z. Ming, C. Zhao, H. Kiriazis, Q. Xu, G.W. Tregear, R.A. Bathgate, X.J. Du, Relaxin remodels fibrotic healing following myocardial infarction, Lab. Invest. 91 (5) (2011) 675–690.

[10] E.D. Lekgabe, H. Kiriazis, C. Zhao, Q. Xu, X.L. Moore, Y. Su, R.A. Bathgate, X.J. Du, C.S. Samuel, Relaxin reverses cardiac and renal fibrosis in spontaneously hypertensive rats, Hypertension 46 (2) (2005) 412–418.

[11] A. Parikh, D. Patel, C.F. McTiernan, W. Xiang, J. Haney, L. Yang, B. Lin, A.D. Kaplan, G.C. Bett, R.L. Rasmusson, S.G. Shroff, D. Schwartzman, G. Salama, Relaxin suppresses atrial fibrillation by reversing fibrosis and myocyte hypertrophy and increasing conduction velocity and sodium current in spontaneously hypertensive rat hearts, Circ. Res. 113 (3) (2013) 313–321.

[12] B. Martin, B. Gabris, A.F. Barakat, B.L. Henry, M. Giannini, R.P. Reddy, X. Wang, G. Romero, G. Salama, Relaxin reverses maladaptive remodeling of the aged heart through Wnt-signaling, Sci. Rep. 9 (1) (2019) 18545.

[13] B. Martin, B.A. Gabris-Weber, R. Reddy, G. Romero, A. Chattopadhyay, G. Salama, Relaxin reverses inflammatory and immune signals in aged hearts, PLoS One 13 (1) (2018) e0190935.

[14] G. Romero, G. Salama, Relaxin abrogates genomic remodeling of the aged heart, Vitam. Horm. 115 (2021) 419–448.

[15] B. Martin, R.R. Vanderpool, B.L. Henry, J.B. Palma, B. Gabris, Y.C. Lai, J. Hu, S.P. Tofovic, R.P. Reddy, A.L. Mora, M.T. Gladwin, G. Romero, G. Salama, Relaxin inhibits ventricular arrhythmia and asystole in rats with pulmonary arterial hypertension, Front Cardiovasc Med 8 (2021) 668222.

[16] C.S. Samuel, C. Zhao, R.A. Bathgate, X.J. Du, R.J. Summers, E.P. Amento, L.L. Walker, M. McBurnie, L. Zhao, G.W. Tregear, The relaxin gene-knockout mouse: a model of progressive fibrosis, Ann. N. Y. Acad. Sci. 1041 (2005) 173–181.

[17] X.L. Moore, S.L. Tan, C.Y. Lo, L. Fang, Y.D. Su, X.M. Gao, E.A. Woodcock, R.J. Summers, G.W. Tregear, R.A. Bathgate, X.J. Du, Relaxin antagonizes hypertrophy and apoptosis in neonatal rat cardiomyocytes, Endocrinology 148 (4) (2007) 1582–1589.

[18] X. Zhang, X. Ma, M. Zhao, B. Zhang, J. Chi, W. Liu, W. Chen, Y. Fu, Y. Liu, X. Yin, H2 and H3 relaxin inhibit high glucose-induced apoptosis in neonatal rat ventricular myocytes, Biochimie 108 (2015) 59–67.

[19] G. Boccalini, C. Sassoli, L. Formigli, D. Bani, S. Nistri, Relaxin protects cardiac muscle cells from hypoxia/reoxygenation injury: involvement of the Notch-1 pathway, FASEB J. 29 (1) (2015) 239–249.

[20] T. Dschietzig, K. Alexiou, H.-T. Kinkel, G. Baumann, K. Matschke, K. Stangl, The positive inotropic effect of relaxin-2 in human atrial myocardium is preserved in end-stage heart failure: role of Gi-phosphoinositide-3 kinase signaling, J. Card. Fail. 17 (2) (2011) 158–166.

[21] T. Dschietzig, S. Teichman, E. Unemori, S. Wood, J. Boehmer, C. Richter, G. Baumann, K. Stangl, Intravenous recombinant human relaxin in compensated heart failure: A safety, tolerability, and pharmacodynamic trial, J. Cardiac Failure 15 (3) (2009) 182–190.

[22] P. Ponikowski, V. Mitrovic, M. Ruda, A. Fernandez, A.A. Voors, A. Vishnevsky, G. Cotter, O. Milo, U. Laessing, Y. Zhang, M. Dahlke, R. Zymlinski, M. Metra, A randomized, double-blind, placebo-controlled, multicentre study to assess haemodynamic effects of serelaxin in patients with acute heart failure, Eur. Heart J. 35 (7) (2014) 431–441.

[23] M. Metra, J.R. Teerlink, G. Cotter, B.A. Davison, G.M. Felker, G. Filippatos, B.H. Greenberg, P.S. Pang, P. Ponikowski, A.A. Voors, K.F. Adams, S.D. Anker, A. Arias-Mendoza, P. Avendano, F. Bacal, M. Bohm, G. Bortman, J.G.F. Cleland, A. Cohen-Solal, M.G. Crespo-Leiro, M. Dorobantu, L.E. Echeverria, R. Ferrari, S. Goland, E. Goncalvesova, A. Goudev, L. Kober, J. Lema-Osores, P.D. Levy, K. McDonald, P. Manga, B. Merkely, C. Mueller, B. Pieske, J. Silva-Cardoso, J. Spinar, I. Squire, J. Stepinska, W. Van Mieghem, D. von Lewinski, G. Wikstrom, M.B. Yilmaz, N. Hagner, T. Holbro, T.A. Hua, S.V. Sabarwal, T. Severin, P. Szecsody, C. Gimpelewicz, Effects of serelaxin in patients with acute heart failure, N. Engl. J. Med. 381 (8) (2019) 716–726.

[24] J.R. Teerlink, G. Cotter, B.A. Davison, G.M. Felker, G. Filippatos, B.H. Greenberg, P. Ponikowski, E. Unemori, A.A. Voors, K.F. Adams Jr., M.I. Dorobantu, L.R. Grinfeld, G. Jondeau, A. Marmor, J. Masip, P.S. Pang, K. Werdan, S.L. Teichman, A. Trapani, C.A. Bush, R. Saini, C. Schumacher, T.M. Severin, M. Metra, Serelaxin, recombinant human relaxin-2, for treatment of acute heart failure (RELAX-AHF): a randomised, placebo-controlled trial, Lancet 381 (9860) (2013) 29–39.

[25] A.I. Agoulnik, I.U. Agoulnik, X. Hu, J. Marugan, Synthetic non-peptide low molecular weight agonists of the relaxin receptor 1, Br. J. Pharmacol. 174 (10) (2017) 977–989.

[26] N. Sasipong, P. Schlegel, J. Wingert, C. Lederer, E. Meinhardt, A. Ziefer, C. Schmidt, K. Rapti, C. Thöni, N. Frey, P. Most, H.A. Katus, P.W.J. Raake, Ligand-activated RXFP1 gene therapy ameliorates pressure overload-induced cardiac dysfunction, Mol. Ther. (2021).

[27] T. Devarakonda, A.G. Mauro, C. Cain, A. Das, F.N. Salloum, Cardiac gene therapy with relaxin receptor 1 overexpression protects against acute myocardial infarction, JACC Basic Transl. Sci. 7 (1) (2022) 53–63.

[28] B. Vogel, H. Siebert, U. Hofmann, S. Frantz, Determination of collagen content within picrosirius red stained paraffin-embedded tissue sections using fluorescence microscopy, MethodsX 2 (2015) 124–134.

[29] D. Kim, G. Pertea, C. Trapnell, H. Pimentel, R. Kelley, S.L. Salzberg, TopHat2: accurate alignment of transcriptomes in the presence of insertions, deletions and gene fusions, Genome Biol. 14 (4) (2013) R36.

[30] B. Langmead, C. Trapnell, M. Pop, S.L. Salzberg, Ultrafast and memory-efficient alignment of short DNA sequences to the human genome, Genome Biol. 10 (3) (2009) R25.

[31] K.F. Au, H. Jiang, L. Lin, Y. Xing, W.H. Wong, Detection of splice junctions from paired-end RNA-seq data by SpliceMap, Nucleic Acids Res. 38 (14) (2010) 4570–4578.

[32] M.D. Robinson, D.J. McCarthy, G.K. Smyth, edgeR: a Bioconductor package for differential expression analysis of digital gene expression data, Bioinform. (Oxford, England) 26 (1) (2010) 139–140.

[33] D.J. McCarthy, Y. Chen, G.K. Smyth, Differential expression analysis of multifactor RNA-Seq experiments with respect to biological variation, Nucl. Acids Res. 40 (10) (2012) 4288–4297.

[34] Y. Chen, A.T.L. Lun, G.K. Smyth, From reads to genes to pathways: differential expression analysis of RNA-Seq experiments using Rsubread and the edgeR quasi-likelihood pipeline, F1000Research 5 (2016) 1438.

[35] K.A. Mullan, L.M. Bramberger, P.R. Munday, G. Goncalves, J. Revote, N.A. Mifsud, P.T. Illing, A. Anderson, P. Kwan, A.W. Purcell, C. Li, ggVolcanoR: A Shiny app for customizable visualization of differential expression datasets, 19 (2021) 5735–5740.

[36] H. Fang, G.P. Brooks, M.L. Rizzo, K.A. Espy, R.S. Barcikowski, A Monte Carlo power analysis of traditional repeated measures and hierarchical multivariate linear models in longitudinal data analysis, J. Mod. Appl. Stat. Methods 7 (1) (2008).

[37] J.D. Molkentin, S.M. Jobe, B.E. Markham, Alpha-myosin heavy chain gene regulation: delineation and characterization of the cardiac muscle-specific enhancer and muscle-specific promoter, J. Mol. Cell. Cardiol. 28 (6) (1996) 1211–1225.

[38] R.A. Bathgate, M.L. Halls, E.T. van der Westhuizen, G.E. Callander, M. Kocan, R. J. Summers, Relaxin family peptides and their receptors, Physiol. Rev. 93 (1) (2013) 405–480.

[39] X.X. Shuai, Y.D. Meng, Y.X. Lu, G.H. Su, X.F. Tao, J. Han, S.D. Xu, P. Luo, Relaxin-2 improves diastolic function of pressure-overloaded rats via phospholamban by activating Akt, Int. J. Cardiol. 218 (2016) 305–311.

[40] O.D. Sherwood, Relaxin's physiological roles and other diverse actions, Endocr. Rev. 25 (2) (2004) 205–234.

[41] C.S. Samuel, F. Lin, M.A. Hossain, C. Zhao, T. Ferraro, R.A. Bathgate, G.W. Tregear, J.D. Wade, Improved chemical synthesis and demonstration of the relaxin receptor binding affinity and biological activity of mouse relaxin, Biochemistry 46 (18) (2007) 5374–5381.

[42] R.J. Bell, L.W. Eddie, A.R. Lester, E.C. Wood, P.D. Johnston, H.D. Niall, Relaxin in human pregnancy serum measured with an homologous radioimmunoassay, Obstet. Gynecol. 69 (4) (1987).

[43] L.V. Bogic, S.Y. Yamamoto, L.K. Millar, G.D. Bryant-Greenwood, Developmental regulation of the human relaxin genes in the decidua and placenta: overexpression in the preterm premature rupture of the fetal membranes1, Biol. Reprod. 57 (4) (1997) 908–920.

[44] T. Dschietzig, C. Richter, C. Bartsch, M. Laule, F.P. Armbruster, G. Baumann, K. Stangl, The pregnancy hormone relaxin is a player in human heart failure, FASEB J. 15 (12) (2001) 2187–2195.

[45] X.J. Du, C.S. Samuel, X.M. Gao, L. Zhao, L.J. Parry, G.W. Tregear, Increased myocardial collagen and ventricular diastolic dysfunction in relaxin deficient mice: a gender-specific phenotype, Cardiovasc. Res. 57 (2) (2003) 395–404.

[46] M.L. Halls, R.A.D. Bathgate, R.J. Summers, Relaxin family peptide receptors RXFP1 and RXFP2 modulate cAMP signaling by distinct mechanisms, Mol. Pharmacol. 70 (1) (2006) 214–226.

[47] M.L. Halls, D.M. Cooper, Sub-picomolar relaxin signalling by a pre-assembled RXFP1, AKAP79, AC2, beta-arrestin 2, PDE4D3 complex, EMBO J. 29 (16) (2010) 2772–2787.

[48] A.M. Svendsen, M. Vrecl, T.M. Ellis, A. Heding, J.B. Kristensen, J.D. Wade, R. A. Bathgate, P. De Meyts, J. Nøhr, Cooperative binding of insulin-like Peptide 3 to a dimeric relaxin family peptide receptor 2, Endocrinology 149 (3) (2008) 1113–1120.

[49] B.S. Chow, M. Kocan, S. Bosnyak, M. Sarwar, B. Wigg, E.S. Jones, R.E. Widdop, R. J. Summers, R.A. Bathgate, T.D. Hewitson, C.S. Samuel, Relaxin requires the angiotensin II type 2 receptor to abrogate renal interstitial fibrosis, Kidney Int. 86 (1) (2014) 75–85.

[50] B.S.M. Chow, M. Kocan, M. Shen, Y. Wang, L. Han, J.Y. Chew, C. Wang, S. Bosnyak, K.M. Mirabito-Colafella, G. Barsha, B. Wigg, E.K.M. Johnstone, M.A. Hossain, K.D. G. Pfleger, K.M. Denton, R.E. Widdop, R.J. Summers, R.A.D. Bathgate, T. D. Hewitson, C.S. Samuel, AT1R-AT2R-RXFP1 Functional crosstalk in myofibroblasts: impact on the therapeutic targeting of renal and cardiac fibrosis, J Am Soc Nephrol 30 (11) (2019) 2191–2207.

[51] C. Wang, A.A. Pinar, R.E. Widdop, M.A. Hossain, R.A.D. Bathgate, K.M. Denton, B. K. Kemp-Harper, C.S. Samuel, The anti-fibrotic actions of relaxin are mediated through AT(2) R-associated protein phosphatases via RXFP1-AT(2) R functional crosstalk in human cardiac myofibroblasts, FASEB J. 34 (6) (2020) 8217–8233.

[52] M.L. Halls, C.P. Bond, S. Sudo, J. Kumagai, T. Ferraro, S. Layfield, R.A. Bathgate, R. J. Summers, Multiple binding sites revealed by interaction of relaxin family peptides with native and chimeric relaxin family peptide receptors 1 and 2 (LGR7 and LGR8), J. Pharmacol. Exp. Ther. 313 (2) (2005) 677–687.

[53] S.Y. Hsu, K. Nakabayashi, S. Nishi, J. Kumagai, M. Kudo, O.D. Sherwood, A. J. Hsueh, Activation of orphan receptors by the hormone relaxin, Science 295 (5555) (2002) 671–674.

[54] R.A. Bathgate, F. Lin, N.F. Hanson, L. Otvos Jr., A. Guidolin, C. Giannakis, S. Bastiras, S.L. Layfield, T. Ferraro, S. Ma, C. Zhao, A.L. Gundlach, C.S. Samuel, G. W. Tregear, J.D. Wade, Relaxin-3: improved synthesis strategy and demonstration of its high-affinity interaction with the relaxin receptor LGR7 both in vitro and in vivo, Biochemistry 45 (3) (2006) 1043–1053.

[55] M.A. Hossain, B.C. Man, C. Zhao, Q. Xu, X.J. Du, J.D. Wade, C.S. Samuel, H3 relaxin demonstrates antifibrotic properties via the RXFP1 receptor, Biochemistry 50 (8) (2011) 1368–1375.

[56] S. Sudo, J. Kumagai, S. Nishi, S. Layfield, T. Ferraro, R.A. Bathgate, A.J. Hsueh, H3 relaxin is a specific ligand for LGR7 and activates the receptor by interacting with both the ectodomain and the exoloop 2, J. Biol. Chem. 278 (10) (2003) 7855–7862.

[57] X. Lian, S. Beer-Hammer, G.M. König, E. Kostenis, B. Nürnberg, M. Gollasch, RXFP1 receptor activation by relaxin-2 induces vascular relaxation in mice via a Gα (i2)-Protein/PI3Kß/γ/Nitric Oxide-coupled pathway, Front. Physiol. 9 (2018) 1234.

[58] C.S. Samuel, C. Zhao, R.A. Bathgate, C.P. Bond, M.D. Burton, L.J. Parry, R. J. Summers, M.L. Tang, E.P. Amento, G.W. Tregear, Relaxin deficiency in mice is associated with an age-related progression of pulmonary fibrosis, FASEB J. 17 (1) (2003) 121–123.

[59] H.F. Nicolaus, T. Klonisch, F. Paulsen, F. Garreis, C1q/TNF-related proteins 1, 6 and 8 are involved in corneal epithelial wound closure by targeting relaxin receptor RXFP1 in vitro, Int. J. Mol. Sci. 24 (7) (2023).

[60] T. Klonisch, A. Glogowska, T. Thanasupawat, M. Burg, J. Krcek, M. Pitz, A. Jaggupilli, P. Chelikani, G.W. Wong, S. Hombach-Klonisch, Structural commonality of C1q TNF-related proteins and their potential to activate relaxin/ insulin-like family peptide receptor 1 signalling pathways in cancer cells, Br. J. Pharmacol. 174 (10) (2017) 1025–1033.

[61] A. Glogowska, U. Kunanuvat, J. Stetefeld, T.R. Patel, T. Thanasupawat, J. Krcek, E. Weber, G.W. Wong, M.R. Del Bigio, C. Hoang-Vu, S. Hombach-Klonisch, T. Klonisch, C1q-tumour necrosis factor-related protein 8 (CTRP8) is a novel interaction partner of relaxin receptor RXFP1 in human brain cancer cells, J. Pathol. 231 (4) (2013) 466–479.

[62] J.M. Peterson, Z. Wei, G.W. Wong, CTRP8 and CTRP9B are novel proteins that hetero-oligomerize with C1q/TNF family members, Biochem. Biophys. Res. Commun. 388 (2) (2009) 360–365.

[63] H. Lei, D. Wu, J.Y. Wang, L. Li, C.L. Zhang, H. Feng, F.Y. Fu, L.L. Wu, C1q/tumor necrosis factor-related protein-6 attenuates post-infarct cardiac fibrosis by targeting RhoA/MRTF-A pathway and inhibiting myofibroblast differentiation, Basic Res. Cardiol. 110 (4) (2015) 35.

[64] K. Nishimura, M. Asakura, S. Hirotani, Y. Okuhara, M. Shirai, Y. Orihara, Y. Matsumoto, Y. Naito, N. Minamino, T. Masuyama, M. Ishihara, Manipulation of beta-adrenergic receptor in pressure-overloaded murine hearts mimics adverse and reverse cardiac remodeling, Biochem. Biophys. Res. Commun. 527 (4) (2020) 960–967.

[65] E.G. Kranias, R.J. Hajjar, Modulation of cardiac contractility by the phospholamban/SERCA2a regulatome, Circ. Res. 110 (12) (2012) 1646–1660.